

Solar Gamma-Ray Evidence for a Distinct Population of > 1 MeV Flare-Accelerated Electrons

GERALD H. SHARE,^{1,2} RONALD J. MURPHY,³ BRIAN R. DENNIS,⁴ AND
JUSTIN D. FINKE⁵

¹ *Astronomy Department, University of Maryland, College Park, MD 20740, USA*

² *TSC, Resident at the Naval Research Laboratory, Washington, DC 20375-5352, USA*

³ *Retired*

⁴ *Emeritis, Solar Physics Laboratory, Code 671, NASA Goddard Space Flight Center, Greenbelt MD 20771, USA*

⁵ *Space Sciences Division, Naval Research Laboratory, Washington, DC 20375-5352, USA*

ABSTRACT

Significant improvements in our understanding of nuclear γ -ray line production and instrument performance allow us to better characterize the continuum emission from electrons at energies $\gtrsim 300$ keV during solar flares. We represent this emission by the sum of a power-law extension of hard X-rays (PL) and a power law times an exponential function (PLexp). We fit the γ -ray spectra in 25 large flares observed by *SMM*, *RHESSI*, and *Fermi* with this summed continuum along with calculated spectra of all known nuclear components. The PL, PLexp, and nuclear components are separated spectroscopically. A distinct origin of the PLexp is suggested by significant differences between its time histories and those of the PL and nuclear components. *RHESSI* imaging/spectroscopy of the 2005 January 20 flare, reveals that the PL and nuclear components come from the footpoints while the PLexp component comes from the corona. While the index and flux of the anisotropic PL component are strongly dependent on the flares' heliocentric angle, the PLexp parameters show no such dependency and are consistent with a component that is isotropic. The PLexp spectrum is flat at low energies and rolls over at a few MeV. Such a shape can be produced by inverse Compton scattering of soft X-rays by 10–20 MeV electrons and by thin-target bremsstrahlung from electrons with a spectrum that peaks between 3 – 5 MeV, or by a combination of the two processes. These electrons can produce radiation detectable at other wavelengths.

Keywords: Sun: corona — Sun: chromosphere — Sun: flares — Sun: electrons —
Sun: X-rays, gamma rays

1. INTRODUCTION

The solar flare γ -ray spectrum is produced when high-energy electrons and ions interact in the solar atmosphere. Magnetic reconnection in the corona is widely believed to initiate flares and release the energy to accelerate these particles to relativistic energies in the corona (e.g. [Chen et al. \(2020\)](#); [Fleishman et al. \(2020\)](#)) and onto magnetic loops anchored in the photosphere ([Holman et al. 2011](#); [Benz 2017](#)). Bremsstrahlung from non-thermal electrons in the corona and chromosphere dominates the well-studied X-ray spectrum $\gtrsim 20$ keV ([Dennis 1988](#); [Krucker et al. 2008b](#); [Holman et al. 2011](#); [Fletcher et al. 2011](#); [Kontar et al. 2011](#); [White et al. 2011](#); [Kontar et al. 2019](#)) and extends into the γ -ray energy range where nuclear contributions to the spectrum become important ([Vestrand 1988](#); [Vilmer et al. 2011](#)). It was known from the early γ -ray measurements in the 1980's by the *Solar Maximum Mission* Gamma Ray Spectrometer (*SMM/GRS*) that electrons can be accelerated to tens of MeV because their steep γ -ray spectrum could be distinguished from the hard π -decay spectrum produced by the interaction of >300 MeV protons deep in the chromosphere ([Forrest et al. 1986](#)).

It has been difficult to unambiguously determine the > 300 keV flare emission produced by electrons, primarily because of the nuclear lines and continuum that also contribute to the γ -ray spectrum in this energy range. Nuclear γ rays were first detected by the *OSO-7* spectrometer from the 1972 August 4 flare ([Chupp et al. 1973](#)). [Suri et al. \(1975\)](#) found a residual MeV continuum after subtracting background and solar nuclear lines at 0.5, 1.6, 2.2, 4.4, and 6.1 MeV, and their instrumental continua. However, using the latest nuclear cross sections available at the time, [Ramaty et al. \(1977\)](#) concluded that almost all of the residual MeV radiation was due to the superposition of broad and narrow nuclear lines that were not taken into account by [Suri et al. \(1975\)](#). The importance of knowing the nuclear contribution in studies of the MeV electron-produced continuum was highlighted by [Vestrand \(1988\)](#) and [Shih et al. \(2009\)](#), who found a close correlation of >300 keV electron bremsstrahlung with both nuclear de-excitation and 2.223 neutron-capture line emissions. Ion acceleration appears to accompany relativistic electron acceleration down to the limiting sensitivity of detectors, thus highlighting the requirement for an accurate knowledge of nuclear-line emission in flares.

The road to this understanding commenced with the seminal work of [Ramaty et al. \(1979\)](#) and led to the detailed studies of particle acceleration onto magnetic loops ([Hua et al. 1989](#); [Murphy et al. 2007](#)), production of the 511-keV positron annihilation line ([Murphy et al. 2005, 2014](#)), broad and narrow nuclear de-excitation lines and unresolved continuum ([Kozlovsky et al. 2002](#); [Murphy et al. 2009, 2016](#); [Tusnski et al. 2019](#)), neutrons and the 2.223 MeV capture line ([Hua & Lingenfelter 1987](#); [Murphy et al. 2012](#)), π -decay γ -rays ([Murphy et al. 1987](#); [MacKinnon et al. 2020](#)), Compton-scattered photons from de-excitation lines and continua ([Murphy & Share 2018](#)), and Compton-scattered photons of 2.223 MeV neutron-capture line γ rays ([Murphy and Share, manuscript in preparation](#)). The

end product of all of this work is an array of nuclear γ -ray spectral templates for each of the processes for different ambient and accelerated particle abundances, flare locations, and ion spectral indices. Access to these templates is provided by OSPEX (Object Spectral Executive)¹ that is available in the SSW IDL software depository².

Using this newly-derived information on nuclear γ -ray production, we began a program to fit the time-integrated spectra from 25 intense nuclear-line flares to determine the ambient and accelerated elemental abundances in the plasma where protons and heavier ions interact. It soon became clear that the broken power-law function commonly used in previous studies to represent the electron-generated γ -ray continuum was inadequate to fit all of the flare spectra. This was in part due to the fact the continuum rolled over at high energies. We therefore replaced the broken power-law with the sum of two continuum components: a Power Law extension of the hard X-rays to MeV energies (PL) and a hard MeV continuum represented by a flat Power Law times an exponential (PLexp). This more generalized form naturally accommodates spectra that harden in the MeV range, such as power laws that break up, and importantly allows for possibility that it is produced by two different sources, such as the spectrally distinct footpoint and coronal emissions observed in the 2005 January 20 flare (Krucker et al. 2008a). The exponential factor accommodates spectra with rollovers at high energy (Ellison & Ramaty 1985). This summed continuum was first used in spectral fits to the 2010 June 12 flare observed by *Fermi*/GBM (Ackermann et al. 2012) and in more recent studies (Kurt et al. 2017; Murphy & Share 2018; Lysenko et al. 2019).

In this paper we discuss the characteristics of the PLexp continuum in solar flares over three decades of intensity. We present compelling evidence that it is a unique component, distinct from both the power-law extension of the hard X-rays and the nuclear γ -rays, and that it reveals a new population of MeV electrons. In §2 we describe the instruments used and our fits to the spectra in 25 γ -ray line flares. In §3 we detail the spectral, temporal, spatial, and directional studies that reveal the distinct origin of the PLexp emission. We discuss how the spectral characteristics of the PLexp component in weak flares and ‘electron-dominated’ episodes (Rieger et al. 1998) differ from those in 25 strong nuclear-line flares in §4. We estimate the spectral characteristics of this new population of MeV electrons in §5 assuming that the PLexp component is produced by thin-target bremsstrahlung and/or inverse Compton scattering in the corona. In §6 we summarize the evidence for these coronal MeV electrons and their possible origins, and suggest that they may explain some puzzling solar observations.

2. FITS TO THE γ -RAY SPECTRA IN LARGE NUCLEAR-LINE FLARES

¹ https://hesperia.gsfc.nasa.gov/ssw/packages/spex/doc/ospex_explanation.htm

² http://www.lmsal.com/solarsoft/ssw_whatitis.html

We use data from four instruments: the *Solar Maximum Mission (SMM)* Hard X-ray Burst Spectrometer (HXRBS) (Orwig et al. 1980) and Gamma Ray Spectrometer (GRS) (Forrest et al. 1980), the *Ramaty High Energy Spectroscopic Imager (RHESSI)* (Lin et al. 2002), and the *Fermi* Gamma Ray Burst Monitor (GBM) (Meegan et al. 2009). The only GRS data that are preserved for use with modern computers are limited to flares observed >300 keV, and the associated backgrounds. Unfortunately, in some cases a portion of the flare or background is missing. Therefore not all of the flares can be studied in their entirety. All of the data are in a format compatible with SSW IDL software and were analyzed with OSPEX. We have identified issues with how the original *SMM* GRS and *RHESSI* detector response matrices (DRMs) accounted for γ rays that do not lose all of their energy in the instrument. This affects some of the nuclear-line studies reported up to the time of the solar γ -ray review by Vilmer et al. (2011). The DRMs of both instruments were corrected and incorporated into OSPEX shortly thereafter. We detail the changes made to the GRS DRM in Appendix A. A normalization error in the Compton component of direct photon interactions accounted for half of the problem in the *RHESSI* DRM, with a coincidence mode issue accounting for the other half (David Smith 2009, private communication).

As we discussed above, we fit >300 keV flare spectra with the sum of a nuclear component and a non-nuclear continuum. The non-nuclear continuum is represented by the sum of two components, 1) a Power Law (PL) function and 2) a Power Law times an exponential (PLexp), rather than the broken power-law function used in previous studies. It has the following form for the photon flux, N , as a function of photon energy, E

$$dN/dE = A_{PL}(E/E_0)^{-S_{PL}} + A_{PLexp}(E/E_0)^{-S_{PLexp}} \exp^{-E/E_R} \quad (1)$$

where A_{PL} and S_{PL} are the amplitude and index of the PL component, A_{PLexp} and S_{PLexp} are the amplitude and index of the PLexp component, E_0 is the normalization energy, (we used 0.3 MeV for the fits in this paper), and E_R is the exponential rollover energy.

For the nuclear component, we use the nuclear γ -ray spectra (Murphy et al. 2009) calculated for the best-fitting elemental and accelerated abundances and ion spectral indices derived from our nuclear studies. Our fits to all the GRS flare spectra and to those *RHESSI* spectra without significant degradation due to radiation damage included the following nuclear components: α - ^4He fusion lines, narrow, broad, and ^3He -induced de-excitation line templates, a 2.223-MeV Gaussian neutron-capture line and templates representing its solar Compton-scattered continuum, and the 511-keV positron annihilation line and positronium continuum. Due to the poorer spectral resolution of the *Fermi*/GBM instrument we included only the 511-keV line, the 2.223-MeV line and its solar scattered component, and narrow- and broad-line templates. The fits also included π -decay emission extending down below 10 MeV in the *RHESSI*

and *Fermi*/GBM spectra and in one flare observed by GRS. This emission comes from interactions of >300 MeV protons accelerated in the impulsive and late phases of flares (Share et al. 2018; Ajello et al. 2021). Because GRS spectroscopy only extends to 8.5 MeV, it is difficult to detect and fit the π -decay component. We only included a π -decay component in our fits to SOL19891019T12:59 where a significant flux of >10 MeV late-phase emission was observed throughout the observation (Share et al. 2022).

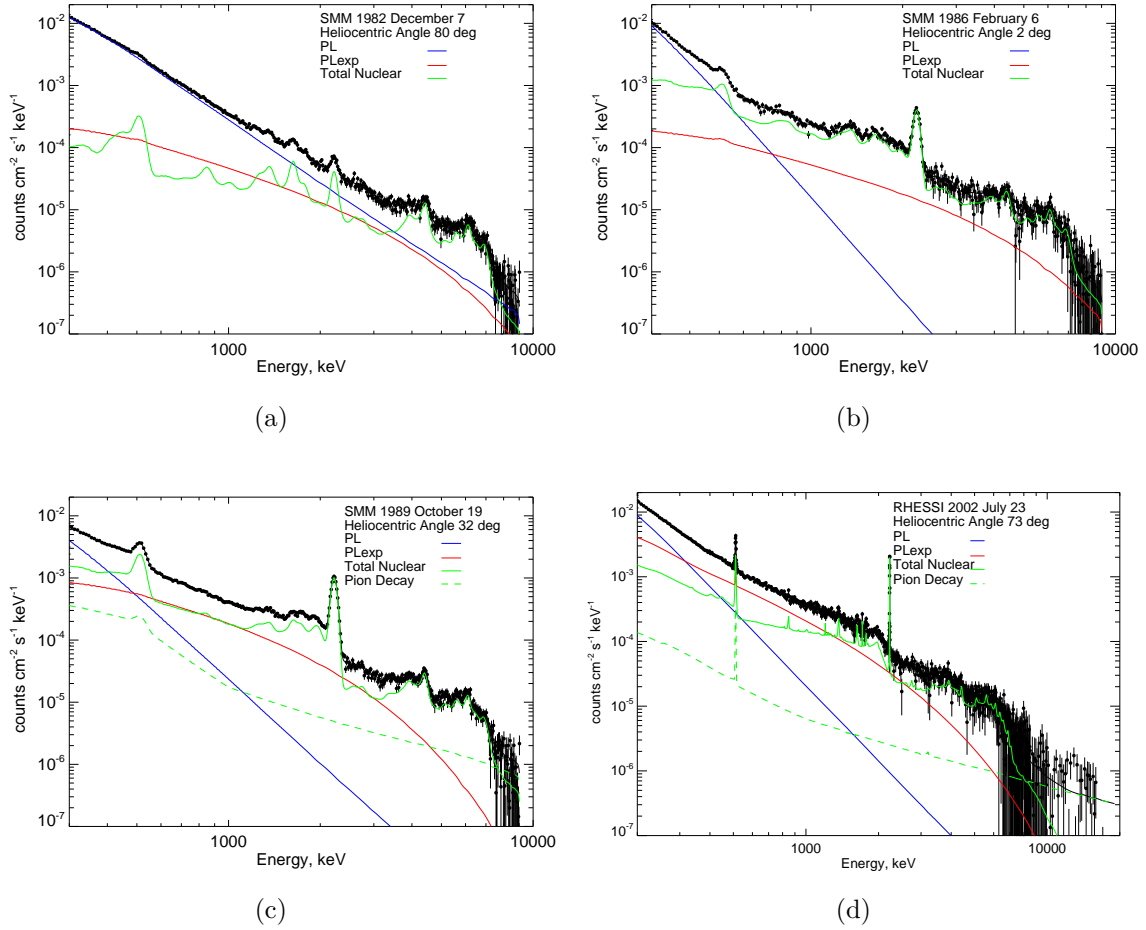


Figure 1. Counts spectra of four flares well fit by Power Law (PL, blue), Power Law times exponential (PLexp, red), and total nuclear (green) components. Also plotted in panels (c) and (d) are the π -decay spectra (dashed green curves) fits to the 1989 October 19 spectrum observed by GRS and the 2002 July 23 spectrum observed by *RHESSI*.

In Figure 1 we plot our fits to the time-integrated count spectra of three large flares observed by GRS and one by *RHESSI*. Counts spectra include instrumental contributions such as escape peaks and continua from partial energy losses. The green curve shows the total nuclear contribution, including the narrow, broad, and unresolved nuclear de-excitation lines, the 511 keV annihilation line, and the 2.223 MeV neutron-capture line and its scattered solar component. The PL (blue) and

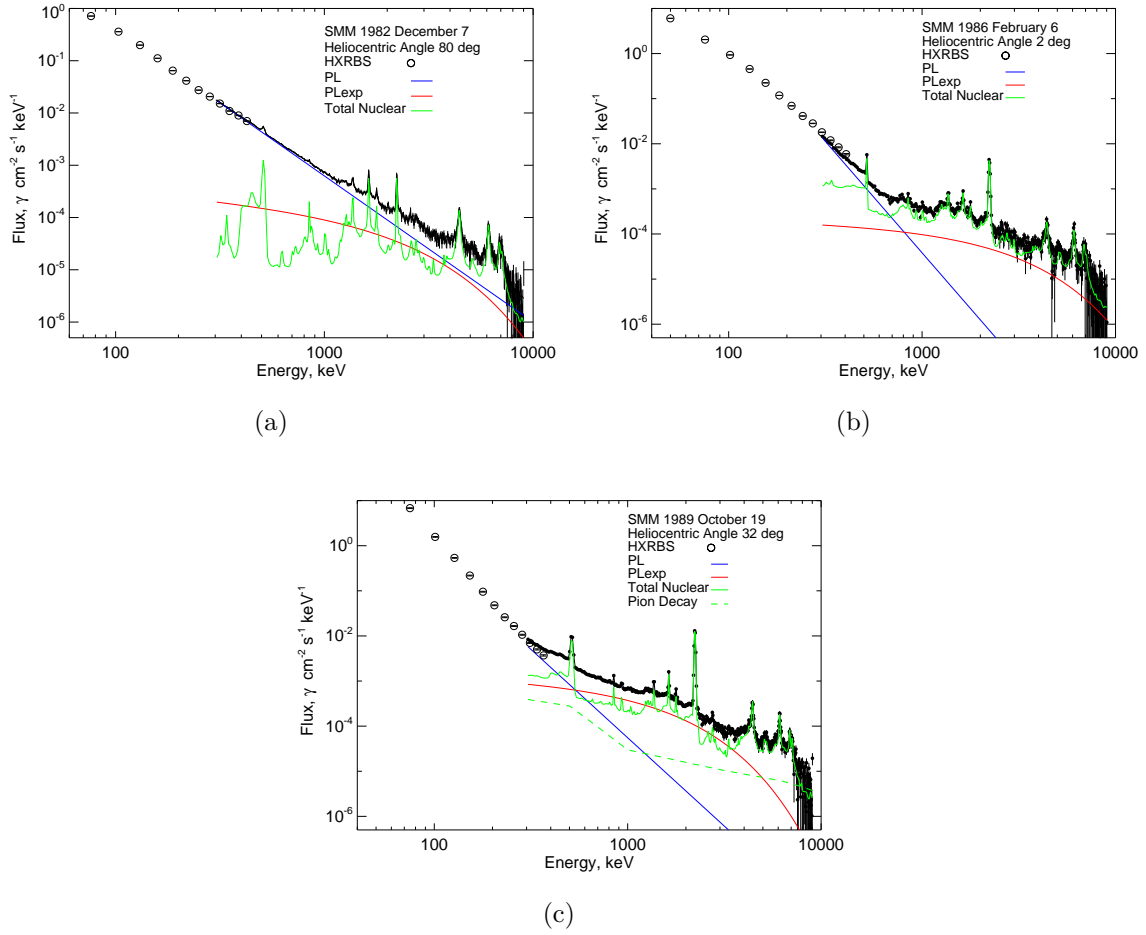


Figure 2. Photon spectra of three flares covering the range from 60 keV to 8.5 MeV using combined data from *SMM* GRS and HXRBS. They are well fit above 300 keV by PL (blue), PLexp (red), and total nuclear (green) components. Also plotted in panel (c) is the π -decay spectrum (dashed green curve) fit to the 1989 October 19 observed by GRS. The plots demonstrate that the PL component observed >300 keV by GRS is the extension of hard X-ray bremsstrahlung. We note that the significance of narrow-lines is exaggerated in plots of photon spectra due to their compliance with the fitted model (Fenimore et al. 1983).

PLexp (red) components are clearly distinguished from each other and from the nuclear component. In panels (c) and (d) we also show the fitted π -decay components (dashed green curves), which have a flat spectrum that is distinguishable from the MeV rollover in the PLexp component.

In establishing the distinct nature of the PLexp, it is important to demonstrate that the PL function is, in fact, the extension of the hard X-ray emission observed below 300 keV. For that reason, in Figure 2 we combine our derived *SMM* HXRBS and GRS photon spectra to cover the energy range from 60 keV to 8500 keV in three flares. In obtaining the HXRBS photon spectra we fit the data with a broken power-law spectral shape. The plots show the excellent agreement between the two instruments in their overlapping energy range and confirm that the PL component derived in GRS fits > 300 keV is indeed the extension of the hard X-ray spectrum.

The plotted components are from our fits to the spectra > 300 keV. We note that there is evidence in some HXRBS spectra for deviations from a single hard X-ray power law that requires further study.

The PL component plotted in Figures 1 and 2 exhibits flare-to-flare variability, displaying striking changes in its hardness and intensity, relative to the PLe_{xp} and nuclear components. As discussed in § 3.3, we attribute this behavior to anisotropy of the electrons producing the PL component. In contrast, the PLe_{xp} component is relatively constant in shape and intensity when compared to the nuclear component. These different behaviors suggest that the PL and PLe_{xp} components have different origins.

The results of our fits to 25 time-integrated flare spectra are listed in Table 1³. We list the following parameters in the numbered columns: (1) the IAU identifier for the flare (Leibacher et al. 2010), where the time is the start time of the accumulation; (2) the duration of the observation; (3) the heliocentric angle of the flare from Sun center; (4)–(6) the parameters (uncertainties) of the fitted PL, amplitude A_{PL} , spectral index S_{PL} , and integrated flux from 0.3 to 10 MeV, Flux_{PL} ; (7)–(10) the parameters (uncertainties) of the fitted PLe_{xp}, amplitude A_{PLexp} , spectral index S_{PLexp} , exponential rollover energy E_R , and integrated flux from 0.3 to 10 MeV, Flux_{PLexp} , and (11) the total narrow plus broad nuclear de-excitation line flux (uncertainties), Flux_{nuc} . The uncertainties of the PLe_{xp} amplitude, index, and rollover energy are large because all were free parameters in the fits and they are strongly correlated with one another and with the PL parameters ($> 90\%$ correlation coefficients). The broad nuclear line and scattered neutron capture line continua are also correlated ($>50\%$) with the PLe_{xp} parameters. The PLe_{xp} uncertainties listed for the fitted parameters provided by OSPEX should include these correlative effects, but may be underestimated.

3. EVIDENCE THAT THE PLEXP CONTINUUM IS A DISTINCT COMPONENT

In the three sections below we present evidence that the PLe_{xp} component has a different origin from the power-law extension of the hard X-ray emission (PL).

3.1. Temporal Variation in Flares

The statistical significance of the fluxes in most of the 27 flares are sufficient to compare the temporal variability of the PL, PLe_{xp}, and nuclear components. We find that the PLe_{xp} component has a different time structure at some point in 20 of the flares. Below, we discuss emissions in seven of the flares where the PLe_{xp} and PL time profiles are distinctly different. In Figure 3 we plot >300 keV fluxes for three GRS flares and one *RHESSI* flare. Although the PLe_{xp} (red-filled circles) fluxes

³ The flares observed by *SMM* on 1982 June 3 and 1984 April 24/25 had significant dead time during the impulsive phase and consequently were not included in the table and ensuing analyses.

Table 1. Details of the Fits to 25 Nuclear-Line Flares

Flare			Power Law			Power Law \times Exp				Nuclear
Date/Time	Dur	Angle	Amp	Index	Flux	Amp	Index	Energy	Flux	Flux
SOL	s	deg	A_{PL}^a	S_{PL}	Flux_{PL}^b	A_{PLexp}^a	S_{PLexp}	E_R^c	Flux_{PLexp}^b	Flux_{nuc}^b
(1)	(2)	(3)	(4)	(5)	(6)	(7)	(8)	(9)	(10)	(11)
19810410T16:45	573	38	2.90(0.18)	3.4(0.2)	0.36(0.04)	0.06(0.17)	0.4(1.7)	4.3(6.3)	0.09(0.25)	0.10(0.02)
19810427T07:56	2425	91	2.73(0.19)	3.4(0.2)	0.34(0.04)	0.37(0.19)	0.9(0.3)	2.7(0.8)	0.22(0.11)	0.19(0.02)
19820709T07:35	197	73	32.40(1.85)	3.2(0.2)	4.52(0.42)	3.46(1.90)	0.8(0.4)	2.0(0.6)	1.97(1.08)	0.51(0.07)
19821126T02:31	262	87	10.94(1.44)	3.6(0.4)	1.27(0.25)	1.92(1.51)	0.7(0.7)	1.3(0.7)	0.81(0.64)	0.27(0.03)
19821207T23:39	2080	80	18.11(0.15)	2.8(0.1)	3.02(0.06)	0.23(0.18)	0.3(0.4)	1.8(0.5)	0.21(0.16)	0.20(0.01)
19860206T06:19	377	2	14.62(0.29)	5.0(0.2)	1.11(0.05)	0.18(0.14)	0.1(0.5)	1.9(0.5)	0.26(0.20)	0.56(0.05)
19881216T08:42 ^e	2766	43	3.30(0.10)	3.4(0.1)	0.40(0.03)	0.16(0.13)	0.5(0.5)	2.9(0.9)	0.15(0.13)	0.15(0.01)
19890306T14:14 ^e	2351	76	18.54(0.13)	2.9(0.1)	2.98(0.03)	0.13(0.06)	0.1(0.3)	1.9(0.3)	0.17(0.08)	0.32(0.01)
19890310T19:03	2767	44	5.16(0.18)	3.4(0.1)	0.66(0.04)	0.34(0.22)	0.8(0.4)	2.4(0.6)	0.22(0.14)	0.14(0.01)
19890317T17:34	410	68	18.25(1.62)	3.4(0.2)	2.25(0.28)	4.53(1.64)	1.3(0.3)	3.5(0.7)	1.89(0.69)	0.62(0.07)
19890503T03:51	590	44	2.87(0.75)	4.1(0.9)	0.28(0.11)	0.77(0.79)	1.5(0.7)	3.8(3.2)	0.27(0.28)	0.13(0.02)
19890816T01:22	803	87	3.19(0.38)	2.4(0.3)	0.68(0.15)	0.28(0.42)	0.3(0.9)	1.7(1.1)	0.28(0.41)	0.17(0.02)
19890817T00:47	2280	90	6.88(0.33)	2.3(0.1)	1.58(0.10)	1.08(0.32)	0.5(0.2)	1.5(0.3)	0.68(0.20)	0.08(0.01)
19890909T09:09	311	30	10.93(0.23)	3.9(0.1)	1.14(0.06)	0.39(0.31)	0.7(0.5)	3.7(1.4)	0.37(0.29)	0.22(0.03)
19891019T12:59	1170	32	6.19(0.38)	3.9(0.3)	0.64(0.07)	1.13(0.28)	0.1(0.3)	1.1(0.2)	0.76(0.19)	0.46(0.02)
19891024T17:57	868	64	13.48(1.09)	3.5(0.2)	1.60(0.20)	1.10(1.04)	0.7(0.8)	1.4(0.8)	0.49(0.47)	0.19(0.02)
19891115T19:31	836	37	6.26(0.26)	3.6(0.2)	0.73(0.06)	0.22(0.25)	0.6(0.7)	2.2(1.1)	0.16(0.18)	0.20(0.03)
20020723T00:27	960	73(35) ^d	13.17(3.00)	3.7(0.7)	1.47(0.53)	4.01(3.33)	0.9(0.8)	1.5(0.9)	1.56(1.30)	0.49(0.05)
20031028T11:08	480	18	30.26(1.54)	4.9(0.5)	2.36(0.32)	12.15(1.51)	0.9(0.1)	2.2(0.2)	6.45(0.80)	1.37(0.12)
20031102T17:16	460	53	52.81(1.23)	3.4(0.1)	6.52(0.39)	1.25(1.33)	0.3(0.6)	1.93(0.6)	1.24(1.32)	1.64(0.16)
20050120T06:44	1080	62	25.70(2.97)	3.3(0.3)	3.59(0.69)	6.90(3.54)	1.0(0.3)	2.8(0.5)	3.38(1.73)	0.61(0.08)
20061206T18:42	1084	60	27.23(2.49)	3.2(0.3)	3.76(0.67)	0.91(1.52)	0.5(0.9)	2.5(1.0)	0.87(1.46)	0.49(0.09)
20100612T00:55	50	61	48.66(1.11)	3.3(0.1)	6.23(0.27)	1.56(1.24)	0.8(0.5)	2.4(0.9)	0.97(0.77)	0.44(0.05)
20140225T00:43	489	78	56.75(4.46)	3.2(0.1)	7.72(0.72)	14.67(4.74)	1.6(0.2)	3.8(0.7)	4.62(1.49)	0.42(0.03)
20170910T15:53	1034	91	5.98(0.57)	2.5(0.1)	1.17(0.15)	0.65(0.59)	0.4(0.8)	1.2(0.6)	0.37(0.34)	0.11(0.02)

NOTE—See Equation 1 for definition of the parameters but note that our energy units here are in MeV for space considerations

$a_{\gamma} \text{ cm}^{-2} \text{ s}^{-1} \text{ MeV}^{-1}$

$b_{\gamma} \text{ cm}^{-2} \text{ s}^{-1}$

^cRollover Energy, MeV

^dField lines appear to be tilted from the vertical by $\sim 40^\circ$ (Smith et al. 2003)

^eSpectral accumulation was delayed until after the time when π -decay emission was detected by the GRS high-energy matrix

followed those of the PL (blue curves) and nuclear components (green-filled circles) early in the 1981 April 27 (panel (a)) and 1989 March 6 (panel (b)) flares, they were

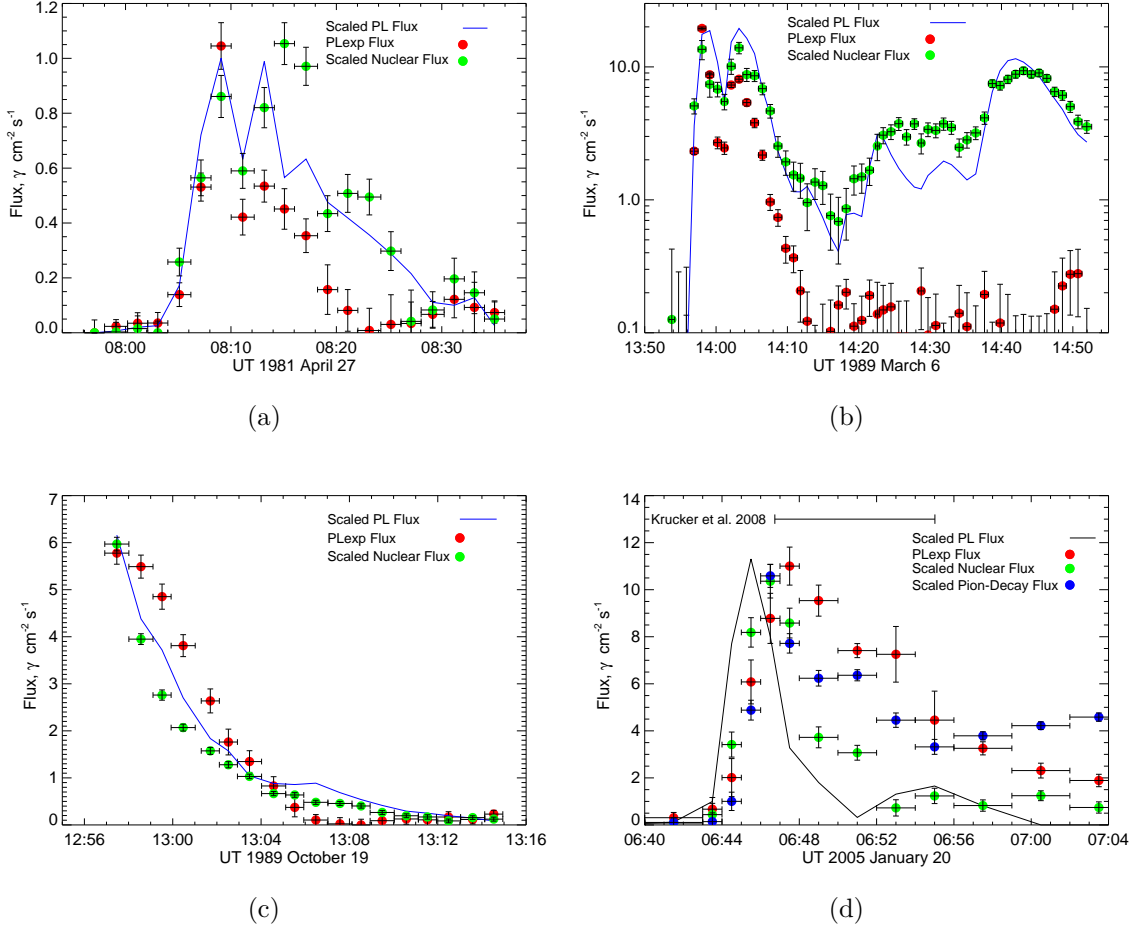


Figure 3. Temporal variations of the fitted power-law (PL), the hard Power-Law \times exponential (PLExp), and the total nuclear de-excitation line fluxes >300 keV in three *SMM* and one *RHESSI* flares suggest a distinct origin of the PLExp component. The > 300 keV PLExp flux is shown on the Y-axis. The PL and nuclear-line fluxes have been scaled for comparison. The π -decay flux time history observed in the 2005 January 20 flare is different from all of the other histories.

significantly weaker at later times. While the PL and nuclear fluxes were falling as observations began after the impulsive phase of the 1989 October 19 flare (panel (c)), the PLExp flux appeared to be rolling over from a peak and fell rapidly relative to them after 13:04 UT. Following the peak of 2005 January 20 flare (panel (d)), both the PL (black curve) and nuclear fluxes fell rapidly while the PLExp flux remained at a high-level for several minutes. We also note the distinctly different π -decay (blue-filled circles) time history in that flare. The significant increase in the PLExp/PL flux ratio following the impulsive phase of the January 20 flare is also clearly seen in three other *RHESSI* flares plotted in Figure 10 of § 6. These significant differences in time histories suggest that the PLExp component has a distinct origin from the PL and nuclear components.

3.2. Location

Our discussion above provides evidence that the PLe_{xp} emission is spectrally and temporally distinct from both the power-law hard X-ray emission and nuclear radiation in flares. This suggests that it has a different origin than the emission from the electron and proton interactions occurring in the chromosphere. [Krucker et al. \(2008a\)](#) discovered a hard coronal source in their *RHESSI* imaging-spectroscopic measurements of the 2005 January 20 flare from 16:46:44 to 16:55 UT (its duration is denoted in Figure 3(d) by the solid black line). It occurred after the PL and nuclear components had both decreased significantly and when the PLe_{xp} component dominated the MeV emission in our spatially-integrated observation.

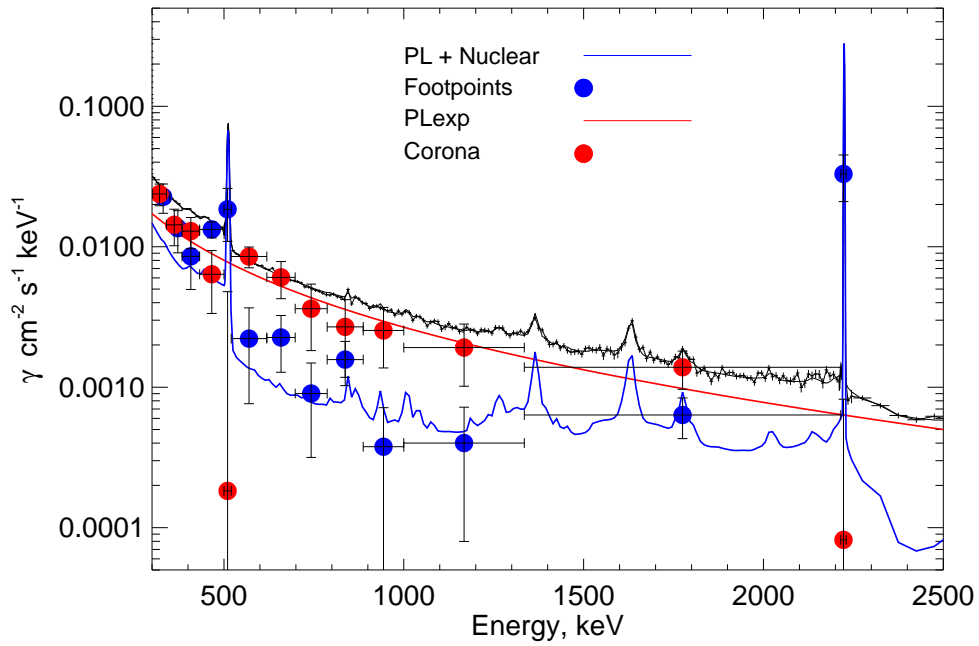


Figure 4. Spatially integrated spectrum (black curve) of the 2005 January 20 flare observed by *RHESSI* rear-detector segments with the fitted PL + nuclear (blue curve) and PLe_{xp} (red curve) components. Footpoint (blue-filled circles; points at 320 and 361 keV have been shifted in energy for visibility) and coronal (red-filled circles) spectra were derived from imaging spectroscopy using *RHESSI*'s rear detector segments. The PLe_{xp} spectral component is consistent with the emission observed from the corona, while the PL and nuclear components are consistent with the emission from the footpoints.

We have improved the *RHESSI* imaging spectroscopy for that time interval and extended its range to energies above 1 MeV. In Figure 4 we plot the derived > 300 keV photon spectra of the radiation from the footpoint (blue-filled circles) and coronal (red-filled circles) sources from 16:46:44 to 16:55 UT. Above 500 keV the coronal emission dominates with the exception of narrow energy bands containing footpoint 511 keV positron annihilation and 2.223 MeV neutron-capture lines. The spatially-integrated photon spectrum (black curve) that we obtained during the same time interval is in good agreement with the sum of the spatially resolved footpoint and

coronal spectra. The spectrum of the fitted PLe_{xp} component (red curve) that was dominant during this time interval (Figure 3(d)) is in remarkably good agreement with the spatially-resolved coronal spectrum, indicating that this high-energy component originated in the corona. The sum of the spatially integrated PL and line fluxes (blue curve) agrees well with emission from the footpoints, consistent with their origins deeper in the solar atmosphere. Our studies using *RHESSI* front detector segments support these conclusions. Although this is the only flare for which there are data to make this spatial and spectral comparison, it provides evidence that the PLe_{xp} emission is spatially distinct from the PL and nuclear radiations emanating from the footpoints, and that its location is consistent with being in the corona.

3.3. Directionality

Bremsstrahlung and inverse Compton scattering by relativistic electrons can produce MeV γ radiation. These radiations are directed along the electron velocity vector and become more tightly beamed as the electron's energy increases (e.g. Petrosian (1985); MacKinnon & Mallik (2010)). Miller & Ramaty (1989) studied the bremsstrahlung produced by an isotropic distribution of >10 MeV coronal electrons injected into a magnetic loop. The radiation pattern from inverse Compton scattering at these energies should be similar. In Figure 5 we plot the calculated angular distributions of γ rays for three different cases of magnetic convergence and turbulence. For a disk flare, $\theta_{obs} = 180^\circ$ and $\cos(\theta_{obs}) = -1$; for a limb flare, $\theta_{obs} = 90^\circ$ and $\cos(\theta_{obs}) = 0$. The amount of magnetic convergence is related to the parameter δ . Below the transition region, the magnetic field strength is assumed proportional to P^δ , where P is the pressure. For coronal and photospheric pressures of 0.2 and 105 dyne cm^{-2} and relevant magnetic field strengths of 100 and 1600 G, respectively, $\delta = 0.2$.

For $\delta = 0$, there is no convergence, and the interacting particle distribution and its high-energy radiation are downward isotropic with almost no radiation escaping from the Sun. For $\delta = 0.2$ but without turbulence, the angular distributions become fan beams peaking at 90° from the downward direction. The strongest escaping radiation is from limb flares ($\cos(\theta_{obs}) = 0$), as seen in Figure 5, where the flux is two orders of magnitude more than that from a disk flare ($\cos(\theta_{obs}) = -1$). When significant turbulence is present in the loops, pitch-angle scattering precipitates electrons into the loss cone, increasing the number of downward-directed electrons. There is little change in the escaping radiation with flare location until the location nears disc center, where there is almost an additional order of magnitude decrease in the escaping flux. This is consistent with the Rieger et al. (1983) finding that the flares observed at these energies were located within $\sim 30^\circ$ of the limb. In a study of the redshifts of nuclear lines as a function flare heliocentric angle Share et al. (2002) found that the angular distribution of the interacting ions is consistent with that from pitch angle scattering in a converging magnetic loop. In the presence of such scattering Miller & Ramaty

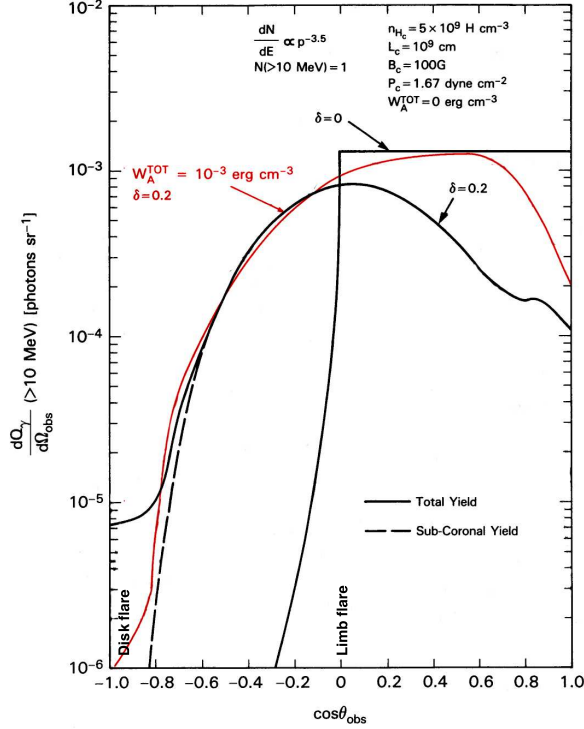


Figure 5. The angular distributions of the bremsstrahlung emission calculated by Miller & Ramaty (1989) from a power-law momentum distribution of electrons injected into a magnetic loop of half length $L-c$ from the corona (density n_h , pressure P_c , magnetic field B_c) for magnetic convergence, $\delta = 0$, and $\delta = 0.2$, with and without MHD turbulence W_k . An observer of a flare at disk center would observe the flux at $\cos\theta_{obs} = -1.0$ and an observer of a flare at the limb would observe the flux at $\cos\theta_{obs} = 0$.

(1989) show in their Figure 13 that the > 10 MeV energy spectrum does not change significantly for angles $> 90^\circ$. This means that one would not expect to observe any changes in the hardness of the spectrum of this high-energy radiation when viewing flares from disk center to the limb, but there would be an orders of magnitude change in intensity.

In contrast to these high-energy calculations, Vestrand et al. (1987) found that the >300 keV bremsstrahlung from flares hardened with increasing heliocentric angle. This hardening for flares observed from disk center to the limb is due to the much broader angular distribution of bremsstrahlung from these lower-energy electrons and the fact that the photon energy decreases with increasing angle from the electron direction. We see a clear example of this hardening with angle when we compare the flat PL spectrum (blue line) shown in Figure 2 (a) for a flare near the solar limb with the steep PL spectra in Figures 2(b) & (c) for flares near disk center.⁴

Details of the angle-dependent characteristics of the PL and PLexp components are revealed using data from Table 1. The significant decrease in the PL index, S_{PL} , >

⁴ It is surprising that the PL component of the 2002 July 23 flare plotted in Figure 2(d) looks similarly steep even though the flare was at 73° . However, Smith et al. (2003) found that the Doppler shifts of nuclear lines in that flare were in better agreement with a flare at a heliocentric angle of $30-40^\circ$, suggesting that the flare loops were significantly tilted toward Earth.

300 keV plotted in Figure 6(a) reveals the strong anisotropy of the electrons in the turbulent magnetic loops. Our linear fit to the index *vs* heliocentric angle for flares at angles $<85^\circ$ is shown by the solid line with the dashed lines showing the uncertainties. S_{PL} decreases from 4.6 ± 0.1 at disk center to 2.4 ± 0.1 at the limb. This decrease is more significant than the 3.4 to 2.7 index change measured by Vestrand et al. (1987). The lower index found by Vestrand et al. (1987) near disk center is due to the hard nuclear-line and PLexp continua that were not accurately subtracted from the spectra. The large uncertainties in S_{PLexp} plotted in Figure 6(b) are due to the strong PL continuum which masks the PLexp component at low energies. A reduction by about a factor of two in S_{PLexp} from disk center to the limb, as found for the PL (solid curve), appears unlikely but is masked by the uncertainties.

In order to determine if S_{PLexp} shows the same decrease with heliocentric angle as S_{PL} , we plot mean (solid blue) and weighted mean (solid red) indices for heliocentric angles from 0° to 50° and from 50° to 85° in panels (a) and (b). For comparison in panel (b) we also plot the expected mean and weighted mean values of S_{PLexp} for heliocentric angles from 50° to 85° (dashed lines) assuming they show the same decrease as S_{PL} . The measured weighted mean value of 1.07 ± 0.10 for S_{PLexp} is inconsistent with the expected value of 0.61 ± 0.06 with $> 99.7\%$ confidence. However, because Miller & Ramaty (1989)'s calculations for > 10 MeV electrons did not show spectral variation with heliocentric angle, it is likely that the expected change in PLexp index would not be as large. The variation of S_{PLexp} appears to be consistent with an isotropic distribution. We note that the weighted mean of S_{PLexp} is < 1 and some are significantly below 1, which is inconsistent with a bremsstrahlung origin. We discuss this issue at the end of § 4 and in § 5.

From the work of Miller & Ramaty (1989) and Vestrand & Ghosh (1987), a better test for anisotropy of the PLexp component is how its flux varies with heliocentric angle. For an anisotropic distribution of 300 – 350 keV bremsstrahlung photons, Vestrand & Ghosh (1987) estimated that fluxes of flares observed near the solar limb would be about a factor seven higher than if they were located near disk center. We plot the measured values of Flux_{PL} *vs* heliocentric angle in Figure 6(c). The large spread in fluxes reflects the flare-to-flare variations such as seen in the intense 2003 October 28 flare observed near a heliocentric angle of 18° . Even with this spread in flux values, there appears to be a significant increase in Flux_{PL} for flares at large heliocentric angles that is comparable to the estimated variation from the work of Miller & Ramaty (1989) that is plotted as a solid curve. Both the mean (solid blue line) and weighted mean (solid red line) fluxes for heliocentric angles from 50° to 85° are about 5 times higher than the means for angles from 0° to 50° . In contrast, there is no significant change in the mean and weighted mean PLexp fluxes for the two ranges of heliocentric angles plotted in Figure 6(d). The weighted mean Flux_{PL} is 0.31 ± 0.06 for 0° to 50° and 0.24 ± 0.07 for 50° to 85° . The dashed blue and red lines show the expected mean and weighted mean (1.45 ± 0.31) fluxes from 50° to

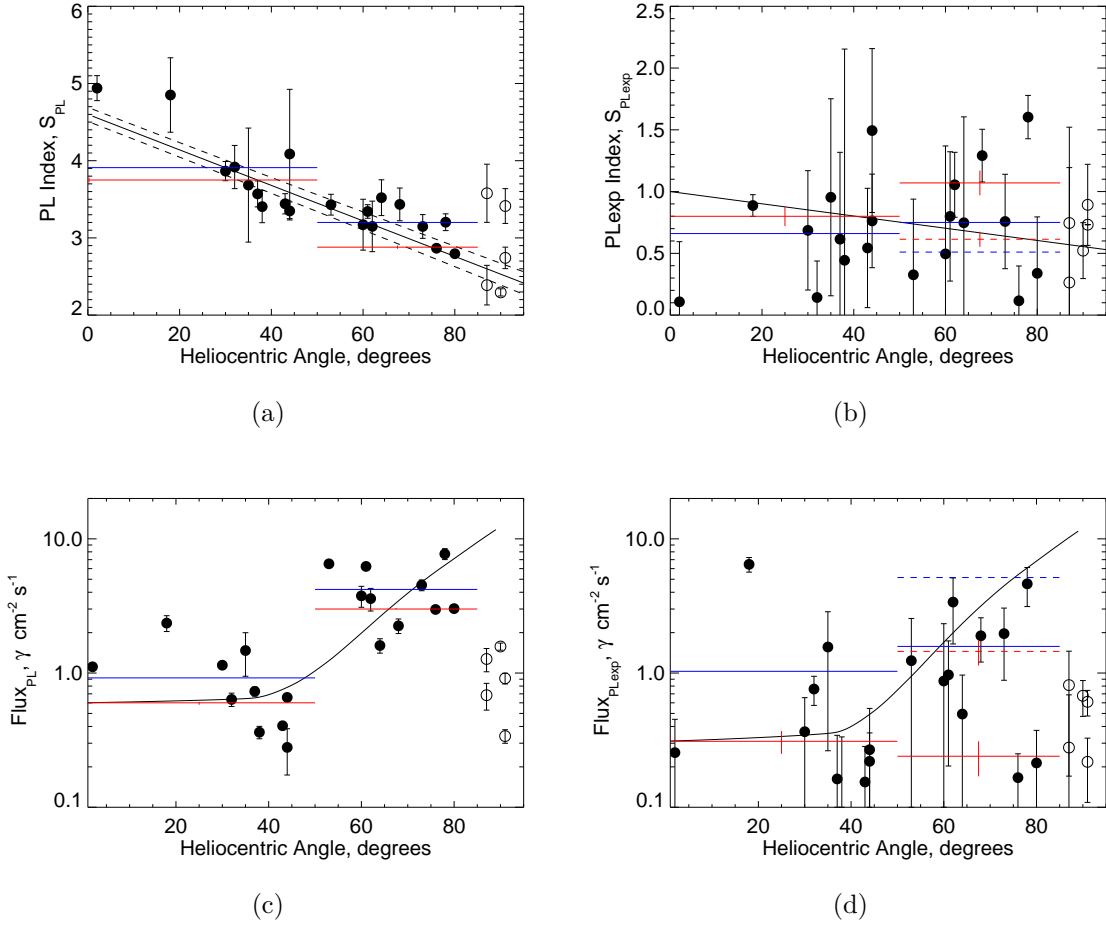


Figure 6. Panels (a) and (b) show the heliocentric angle dependence of the PL index, S_{PL} , and PLeXP index, S_{PLexp} . The best fit S_{PL} linear variation and $\pm 1\sigma$ uncertainties is shown by the solid and dashed lines, respectively in panel (a). This variation is shown by the solid line in panel (b). Panels (c) and (d) show the heliocentric angle dependences of Flux_{PL} and Flux_{PLexp} . The heliocentric variation for bremsstrahlung from > 10 MeV electrons calculated by Miller & Ramaty (1989) is plotted as solid curves in both panel. Means (solid blue lines) and weighted means (solid red lines with uncertainties) of the measured values from 0° to 50° and 50° to 85° are plotted in all four panels. The dashed lines from 50° to 85° in panels (b) and (d) are the estimated means (blue) and weighted means (red) based on the variation observed in panels (a) and (c), respectively. We restricted our fits to angles $< 85^\circ$ (filled circles) due to attenuation effects in flares near the limb (open circles). The high fluxes near 18° came from the intense 2003 October 28 flare that was observed by RHESSI after the impulsive phase.

85° had they increased by the same factors as found for Flux_{PL} plotted in panel (c). The heliocentric variation in Flux_{PLexp} is consistent with an isotropic distribution and is inconsistent with the large change in Flux_{PL} vs heliocentric angle with $> 99.7\%$ confidence.

From the work of Miller & Ramaty (1989), electrons producing such an isotropic distribution would likely radiate from the corona and not from the footpoints. This

is consistent with the coronal location of the PLe_{xp} component in the 2005 January 20 flare.

4. SPECTRAL CHARACTERISTICS OF THE PLEXP COMPONENT

Three parameters define the PLe_{xp} component: its power-law index, S_{PLexp} , its rollover energy, E_R , and its flux relative to the PL component, $\text{Flux}_{PLexp}/\text{Flux}_{PL}$. Table 1 lists the parameters and their uncertainties that provide these values in the 25 strong nuclear line flares that we studied. In order to expand the dynamic range of our study we included ‘electron-dominated’ episodes (Rieger et al. 1998), discussed in Appendix B, and weak solar flares, discussed in Appendix C. These events extended the dynamic range of the flare fluxes that we studied to almost three orders of magnitude (Appendix D).

The measured indices of the PLe_{xp} component, S_{PLexp} , in the 25 large flares are displayed in Figure 6(b). They are consistent with values of ~ 1 or less. We find that the same is true for ‘electron-dominated’ episodes. The fitted index for weak flares is 0.5 ± 0.4 . Thus the PLe_{xp} index is consistent with values of $\lesssim 1$ for flares over three orders of magnitude in intensity. If the PLe_{xp} emission is due to bremsstrahlung, S_{PLexp} cannot be < 1 , but its measurement is compromised by the presence of the strong PL component. Early in the 2005 January 20 flare, between 06:44 and 06:46:44 UT, when the PL component was strong, we measured a S_{PLexp} value of 1.0 ± 0.3 . However, later in the flare from 06:46:44 to 06:55 UT, during the time when we imaged the source and when the PL component was weak, we measured a value of 1.39 ± 0.06 , totally consistent with a bremsstrahlung origin. In § 5.2 we find that the spectra in the 17 flares studied can be fit with thin target bremsstrahlung instead of the PLe_{xp} function with a $> 85\%$ probability. Thus a bremsstrahlung origin for the PLe_{xp} component cannot be ruled out.

The number distribution of rollover energies, E_R , for large nuclear-line flares, plotted as filled green circles in Figure 7(a), peaks at ~ 1.5 MeV, extends up to ~ 5 MeV, and has a mean of 2.2 MeV. In contrast, the E_R distribution of the ‘electron-rich’ episodes is much flatter with a mean value four times higher. For weak flares, the fitted rollover energy of 890 ± 40 keV (blue arrow) is less than any energy found in large flares.

In Figure 7(b) we plot the number distribution of PLe_{xp} to PL flux ratios > 300 keV, $\text{Flux}_{PLexp}/\text{Flux}_{PL}$. We corrected the anisotropic Flux_{PL} to a heliocentric angle of 80° using a fit to the data plotted in Figure 6(c). Corrected to this heliocentric angle, the radiation from a broad downward angular distribution of electrons would be effectively isotropic. We restricted our study to flares $< 85^\circ$ to avoid effects due to attenuation of the PL footpoint emission at the limb. For large flares, the $\text{Flux}_{PLexp}/\text{Flux}_{PL}$ distribution peaks near 0.05, extends up to ~ 0.5 , and has a mean of 0.15. Thus the > 300 keV flux in the PLe_{xp} component is typically less than $\sim 20\%$ of the > 300 keV flux in the PL component for large flares. The $\text{Flux}_{PLexp}/\text{Flux}_{PL}$ distribution for the

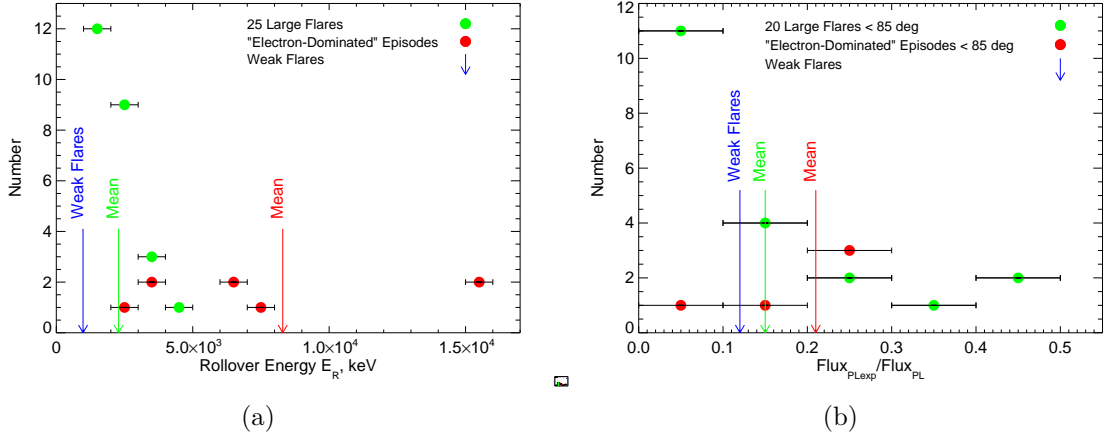


Figure 7. Panel (a): Number distributions of the exponential rollover energy (E_R) for 25 nuclear-line flares (green filled circles) and 8 ‘electron dominated’ episodes [Rieger et al. \(1998\)](#) (red filled circles). Panel (b): Number distribution of the $\text{Flux}_{PLexp}/\text{Flux}_{PL}$ ratio > 0.3 MeV, after correcting the anisotropic Flux_{PL} for heliocentric angle, for 20 flares and 5 ‘electron dominated’ episodes occurring at heliocentric angles $< 85^\circ$. The green and red vertical arrows mark the mean values for the large flares and ‘electron dominated’ episodes, respectively. The blue vertical arrows denote the fitted values for the sum of 48 weak flares.

five ‘electron-rich’ episodes at heliocentric angles $< 85^\circ$, red-filled circles, is flat and has a mean value $\sim 40\%$ higher than that in the large flares. The $\text{Flux}_{PLexp}/\text{Flux}_{PL}$ ratio in weak flares (blue arrow) is only $\sim 20\%$ lower than the mean value found for large flares.

Thus, the rollover energy, E_R , exhibits the most significant difference, varying from a low of ~ 0.9 MeV in weak flares to a mean value of 2.2 MeV in nuclear-line flares and to significantly higher values in ‘electron-dominated’ flares. The $\text{Flux}_{PLexp}/\text{Flux}_{PL}$ ratio follows the same increasing trend but not as strikingly.

5. ELECTRON SPECTRUM PRODUCING THE MEV GAMMA-RAY CONTINUUM

We have identified a solar-flare MeV γ -ray continuum that is temporally distinct from both the power-law extension of the hard X-ray emission and nuclear emission. We have provided evidence that the continuum is consistent with being isotropic and thus not likely to originate in the footpoints. In fact, imaging spectroscopic measurements during the 2005 January 20 flare indicates that it originates in the corona. We have represented its spectrum by a power law times an exponential, PLexp (see Equation 1), where the index of the power-law is typically $\lesssim 1$ and the exponential rollover energy, E_R , ranges from about 1 to 5 MeV in large nuclear line flares. There are two primary mechanisms by which electrons can produce MeV γ rays: inverse Compton scattering and bremsstrahlung. Below we discuss these processes, how well they are able explain the features of the PLexp component, and the characteristics of the electron spectra that would explain the observations.

5.1. *Electron Compton Scattering of Flare X-rays*

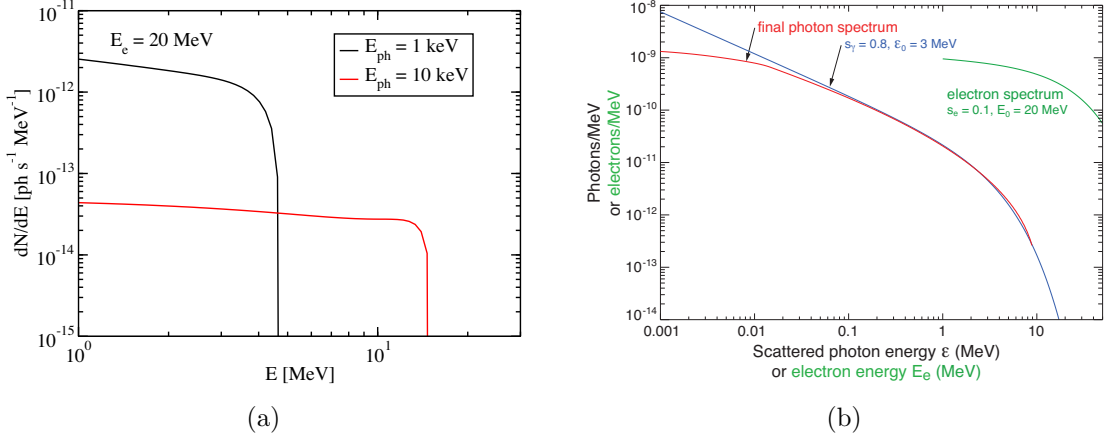


Figure 8. (a) Spectra produced when isotropic 20 MeV electrons Compton scatter an isotropic population of 1 and 10 keV X-rays to MeV energies. (b) An electron spectrum in the shape of a power law with index 0.1 and exponential rollover energy of 20 MeV (green curve) will produce a γ -ray spectrum (red curve) consistent with a PLeXP with index of 0.8 and 3 MeV rollover energy (blue curve).

Flat flare spectra at hundreds of keV energies, such as we observe in the PLeXP component, prompted researchers to consider inverse Compton scattering as an alternative to bremsstrahlung (Krucker et al. 2008b). Such emission is expected to dominate at low coronal mass densities and high-electron energies. MacKinnon & Mallik (2010) made detailed calculations of the emission produced when electrons and positrons with energies reaching 100 MeV up-scattered optical and EUV photons. Chen & Bastian (2012) refined these calculations and extended them to include scattering of soft X-rays emitted during flares. Using the work of Jones (1968) and Blumenthal & Gould (1970), we calculated γ -ray spectra produced when isotropic distributions of high-energy electrons Compton scatter off isotropic photon distributions. In Figure 8(a) we plot the spectrum produced when 20 MeV electrons scatter 1 and 10 keV X-rays. We see that 20 MeV electrons Compton scatter 1 keV X-rays to produce a flat spectrum with a sharp rollover above 4 MeV. A photon spectrum that better reflects the shape of the PLeXP component that we observe in nuclear-line flares would be produced by an electron distribution of the form

$$n(E_e) \propto E_e^{-s_e} \exp -(E_e/E_0) . \quad (2)$$

where n is the number flux of electrons with energy E_e , s_e is the index of the power-law function and E_0 is the exponential rollover energy. An example of such an electron spectrum with $s_e = 0.1$ is plotted in Figure 8(b) along with the resulting photon spectrum that would be produced by inverse Compton scattering of soft X-rays. This photon spectrum is consistent with a PLeXP spectrum with an index $<$

1, which raised questions about a bremsstrahlung origin that we discussed in § 4. It is beyond the scope of this paper for us to fit the data to obtain the best electron spectral distribution, but we expect that spectrum to rollover at energies below 20 MeV.

5.2. *Electron Thin-Target Bremsstrahlung*

Here we determine whether thin-target bremsstrahlung can produce the flat spectrum represented by the PLe_{xp} component, and determine the characteristics of the electron spectrum. We use the SSWIDL OSPEX ‘thin2’ function to fit the MeV continuum. Unfortunately, only electron-ion (e-i) bremsstrahlung is incorporated in ‘thin2’. Kontar et al. (2007) showed that an upward break (change of ~ 0.4 in index) in the power-law spectrum in the 2005 January 17 flare can be explained by including electron-electron (e-e) bremsstrahlung. However, this amount of hardening is too small to account for the PLe_{xp} component discussed in this paper. We find that including e-e bremsstrahlung in ‘thin2’ would decrease the estimated electron flux by about a factor of two but has a less significant impact on determination of the shape of the electron spectrum (Haug (1998); Oparin et al. (2020) and Ivan Oparin [2024, private communication]). The ‘thin2’ function assumes that the electrons have a broken power-law energy spectrum with the normalization factor (electron flux > 300 keV \times source density \times source volume), the break energy, and the indices below and above the break energy as free parameters.

We were able to fit the spectra and obtain well-defined parameters in 17 nuclear-line flares using the ‘thin2’ function and the same power-law (PL) and nuclear-line photon components used for the PLe_{xp} fits in §2. Thus, bremsstrahlung is a viable origin for the hard PLe_{xp} component even though the spectral fits give a mean index $\lesssim 1$ in our studies in § 3.3. We have compared the quality of fits for the thin-target origin with those obtained in § 2 for the PLe_{xp} component. Thin-target spectral fits have a mean probability that is 87% of PLe_{xp} fits. The probabilities range from 0.07 to 1.77. It is surprising that the worst thin-target fit is for the 2014 February 25 flare that has the steepest PLe_{xp} index. Our studies indicate that uncertainties in the PL component allow for thin target emission in spite of the fitted hardness of the PLe_{xp} component (also see § 4). When using thin-target bremsstrahlung in the fits the PL spectral index softened by 0.06 ± 0.02 and its flux decreased by 3.3 ± 1.0 %. Thus the presence of the strong PL component affects the determination of the PLe_{xp} index as we found in § 4 where the index had a value of 1.0 ± 0.3 when the PL intensity was strong and a value of 1.39 ± 0.06 when it was weaker.

While the electron break energy and index above that energy were well determined in all of the thin-target fits, we needed to perform a χ^2 minimization analysis to reliably constrain the index below the break energy. We did this by manually changing its value while allowing all the other parameters to vary. We plot the results of these fits in Figure 9. All of the power-law indices below the break energy in panel (a) are

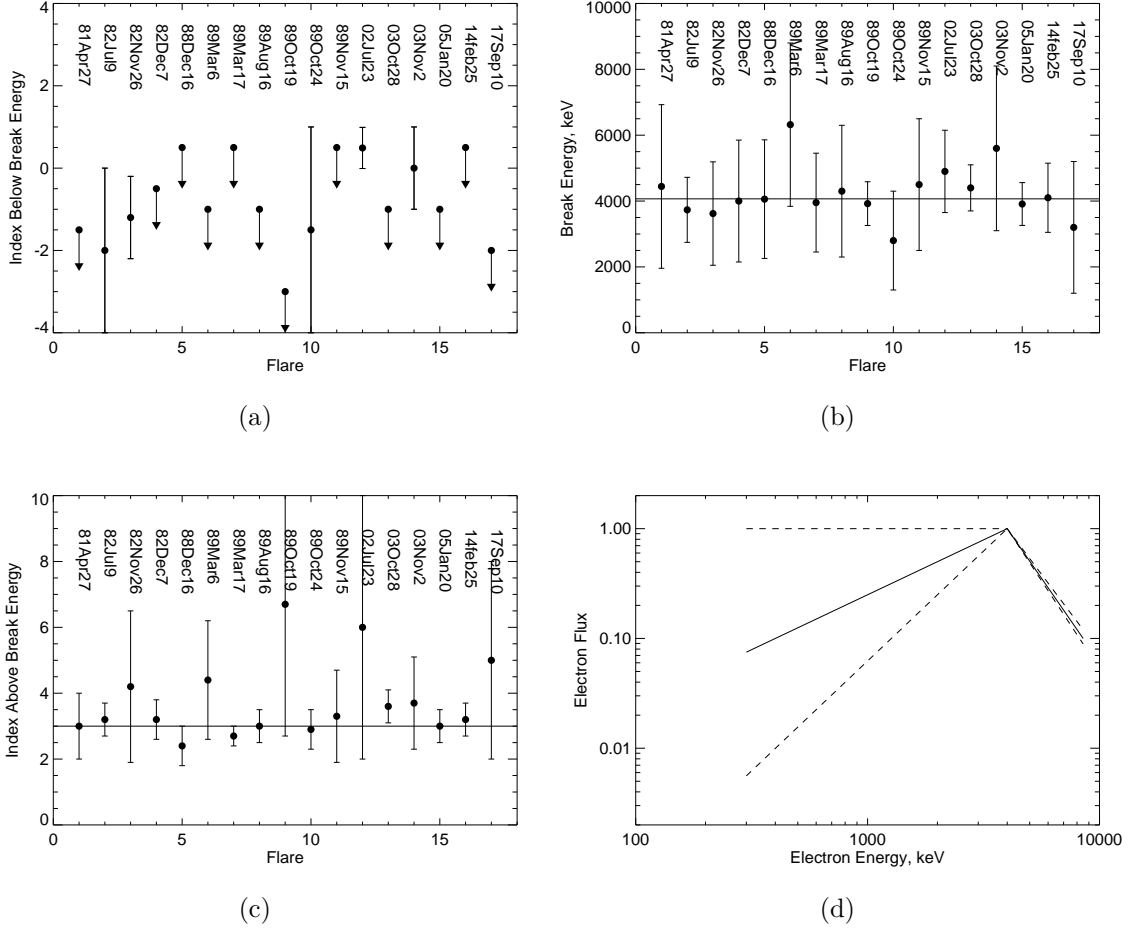


Figure 9. Spectral characteristics of the new electron population in 17 nuclear-line flares assuming that the PLe_{exp} continuum is produced by thin-target bremsstrahlung. The modeled electron spectrum has the shape of a broken power law. Panel (a) shows the fitted indices below the break energy, panel (b) shows the fitted break energies, and panel (c) shows the fitted indices above the break energy. Panel (d) shows a representation of the broken power-law electron spectrum for this model with a mean 4 MeV break energy. Break energies in the fitted flare spectra range between 3 – 5 MeV and the dashed lines show the uncertainties in the fitted indices.

consistent with rising or flat electron spectra, while all of the power-law indices above the break energy are consistent a falling spectrum with a weighted mean index of 3.0 ± 0.2 . Given the large uncertainties, all of the break energies in panel (b) are consistent with their weighted mean of 4.1 ± 0.3 MeV. Although a mono-energetic distribution of electrons can fit the data in a few flares, it generally produced significantly worse fits than a peaked distribution because the observed spectra require photons above the electron break energy.

In Figure 9(d) we plot a representation of the MeV electron spectrum based on the fitted parameters plotted in the other three panels of the figure. The spectrum is flat or rises to a peak energy near 4 MeV and then falls with a power-law index of about 3 at higher energies. We also fit the summed spectrum of 48 weak flares with

thin-target bremsstrahlung. The average break energy for these flares is consistent with 4 MeV, the spectral index of 0.5 ± 0.5 below the break energy is comparable to the steepest observed in the large flares, and the power-law index of 6 ± 2 above the break energy is steeper than the mean in the large flares.

6. SUMMARY AND DISCUSSION

Although solar-flare hard X-ray emission has been well studied, understanding the electron-produced γ -ray emission at energies > 300 keV has been more difficult. One of the obstacles has been the contribution from nuclear γ rays. In a study of 25 nuclear-line flares, significant improvements in our understanding of both nuclear γ -ray line production and instrument performance have allowed us to reveal a distinct flat MeV γ -ray continuum represented by a power law times an exponential (PLexp) function. The spectral fits reliably separate this component from the power-law (PL) extension of hard X-ray emission that dominates solar spectra at lower energies and from the nuclear γ -ray emission at higher energies.

While the time history of the nuclear-line flux typically follows that of the > 300 keV PL emission with a small delay, the time history of the PLexp component shows significant differences in 20 of the intense solar flares in our study. We plot these differences for seven of the flares in Figures 3 and 10. This suggests that the PLexp emission may originate from a different source of accelerated electrons than the hard X-rays. During the time interval in the 2005 January 20 flare when the PLexp emission was dominant, Krucker et al. (2008a) used *RHESSI* imaging spectroscopy to reveal a coronal source of 250–800 keV hard X-rays with a spectrum that was significantly harder than the emission from the footpoints. We extended their studies to cover a broader range of energies and showed that the spatially-integrated PLexp spectrum is in good agreement with the spectrum of these coronal γ -rays, while the sum of the spatially-integrated PL and nuclear-line spectra is consistent with the spectrum observed from the flare footpoints. Thus, at least in this one flare where imaging data are available, the PLexp component is found to originate in the corona.

Our study of the heliocentric-angle dependence of the PLexp index, rollover energy, and flux $\text{Flux}_{\text{PLexp}}$ in the strong nuclear-line flares indicates that the PLexp radiation is consistent with being isotropic. This contrasts with the anisotropic nature of the PL emission revealed by the dependence of its index and flux on the flare’s heliocentric angle. The PLexp spectrum is flat at low energies with indices that are consistent with $\lesssim 1$. The distribution of its rollover energies peaks near 1.5 MeV, extends up to ~ 5 MeV, and has a mean value of 2.2 MeV. The > 0.3 MeV flux in the PLexp component is typically less than $\sim 20\%$ of the heliocentric-angle corrected flux in the PL component.

In a study of flares nearly 100 times weaker (see Appendices C & D) than the 25 strong nuclear-line flares we find a similarly hard low-energy PLexp spectrum and a flux 20% smaller relative to the PL. Significantly, we measure a rollover energy of

~ 900 keV that is more than a factor of two smaller than the mean rollover energy found in the large flares. In contrast, the mean PLe_{xp} rollover energy for ‘electron-dominated’ episodes (Rieger et al. 1998) is more than a factor of three larger than in the large nuclear-line flares, while its flux relative to the PL flux is $\sim 30\%$ higher.

We consider two possible origins for this hard PLe_{xp} component: Compton scattering and thin-target bremsstrahlung. Compton scattering of a distribution of 1 keV flare X-rays by isotropic electrons with flat power-law spectra (index ~ 0.1) and rollover energies between 10 and 20 MeV can produce spectra consistent with the observed PLe_{xp} component, including indices $\lesssim 1$.

While such a flat spectrum is a concern for a bremsstrahlung origin, we nevertheless obtained thin-target fits with comparable probabilities to those using the PLe_{xp} function. This is primarily due to the intense PL component and its affect on the fits. We characterized the spectrum of electrons producing the PLe_{xp} spectrum via thin-target bremsstrahlung. (We note that because our fitting routine only includes electron-ion (e-i) bremsstrahlung, it overestimates the flux of the electrons by about a factor two but does not significantly affect the derived shape of the electron spectrum.) Our fits reveal that the electron spectrum at energies above 300 keV is flat or rises to a peak between 3 and 5 MeV and then falls at higher energies.

Such a spectrum suggests the depletion of low-energy accelerated electrons and/or the presence of relatively persistent ~ 4 MV electric fields in the corona during flares. Electric-field acceleration of electrons in the solar environment has been under study for decades (e.g. Holman (1985); Holman & Benka (1992)). Litvinenko (2000) showed that MV electric field strengths can be produced in reconnecting current sheets in the corona near singular lines of magnetic field where the electric and magnetic fields are co-aligned. Recently, reconnection electric fields of $\sim 4,000$ V m⁻¹ were inferred near the X point from imaging microwave observations (Fleishman et al. 2020; Chen et al. 2020). Similarly-peaked electron spectra but from DC potential drops of 10 kV in the Earth’s auroral zone were referred to by Lin & Schwartz (1987) in their paper on solar hard X-rays bursts.

The hard population of coronal electrons revealed in this study may be detectable by observations made at other wavelengths. Bai & Ramaty (1976) calculated the microwave spectrum from an ~ 4 -MeV exponential-shaped distribution of electrons and showed that it could produce a flux of synchrotron radiation observable at frequencies above 30 GHz. Kaufmann et al. (2004) discovered a new submillimeter component in flares with a steeply-rising spectrum at energies above 200 GHz. Such emission can be produced by a variety of mechanisms (Silva et al. 2007; Trotter et al. 2008; Krucker et al. 2013), including synchrotron emission (Bastian et al. 1998) and thermal bremsstrahlung from an optically thick source (Ohki & Hudson 1975). The ~ 3 -15 MeV population of electrons suggested by our study have cyclotron frequencies of hundreds of GHz in coronal magnetic fields and thus could also produce this submillimeter radiation via synchrotron emission.

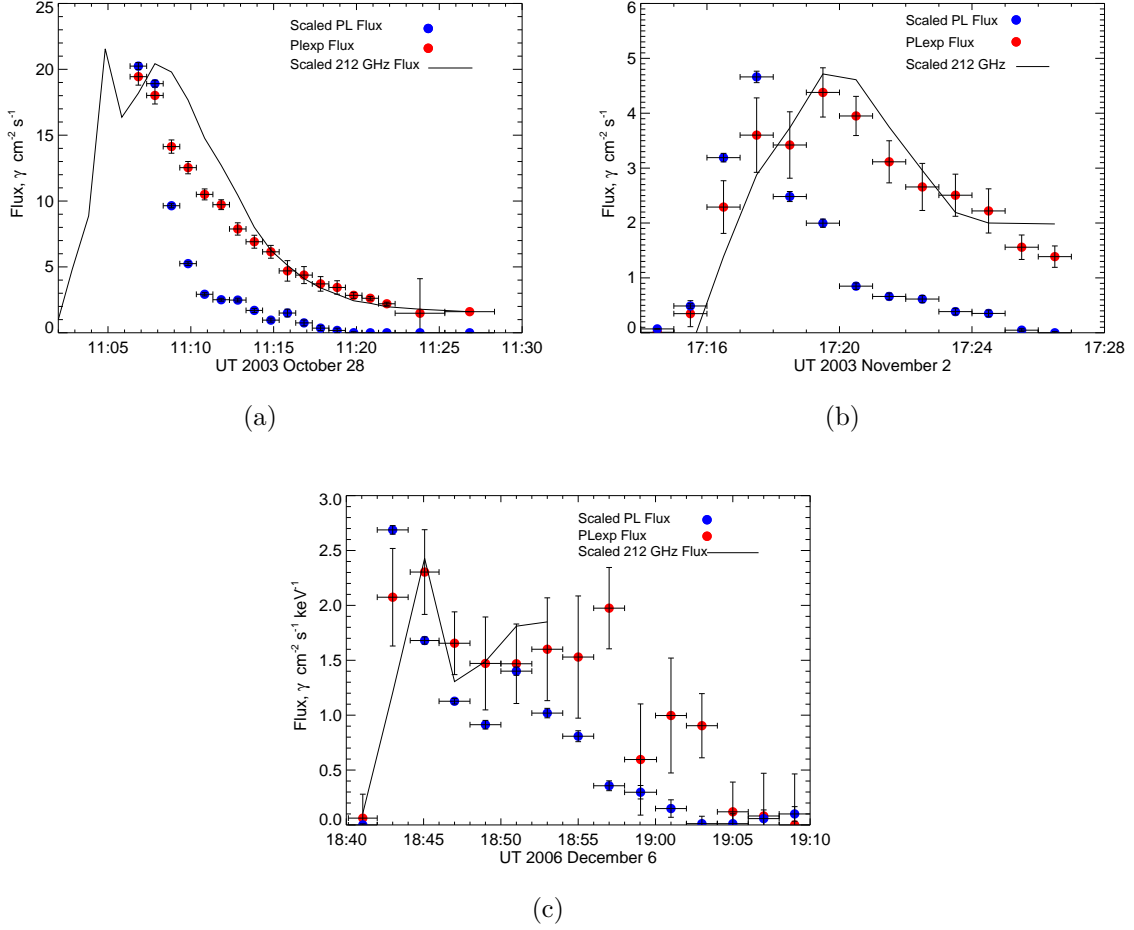


Figure 10. Comparison of the time histories of the PL and PLeXp fluxes in γ -ray spectra and the submillimeter fluxes in the 2003 October 28 (Lüthi et al. 2004), 2003 November 2 (Silva et al. 2007), and 2006 December 6 (Kaufmann et al. 2009) solar flares observed by *RHESSI*.

In Figure 10 we compare the time histories of observed submillimeter fluxes (solid black curves) with the PL, (blue-filled circles) and PLeXp (red-filled circles) fluxes in three flares where joint measurements were made. Both the PLeXp and submillimeter emissions peak later and last longer than the PL emission. In fact, the time histories of the PLeXp and submillimeter fluxes in the 2003 November 2 are remarkably similar. Thus, it is possible that synchrotron emission from the coronal MeV electrons found in the γ -ray studies may be responsible for the rising spectrum of submillimeter emission observed in some flares. In Appendix E we speculate that some of the MeV electrons penetrate deep into the chromosphere to heat the plasma to temperatures of $\sim 5 \times 10^5$ K, thereby producing submillimeter radiation and explaining puzzling γ -ray observations.

1 We mourn the loss of our colleague Richard Schwartz, who led the development of
 2 the OSPEX analysis system that made our analysis of γ -ray data from *SMM*, *RHESSI*,
 3 and *Fermi* possible. Kim Tolbert played a key role in supporting our OSPEX studies
 4 and providing the Fermi solar data from the publicly available NASA archive. J.D.F.
 5 is supported by the Office of Naval Research. We value our discussions with Jeff Reep,
 6 Gregory Fleishman, Ivan Oparin, Albert Shih, Edward Kontar, and the support from
 7 our colleagues at the Naval Research Laboratory. We especially thank an anonymous
 8 referee whose comments prompted us to make the paper more readable and focussed.

APPENDIX

A. *SMM*/GRS INSTRUMENT RESPONSE

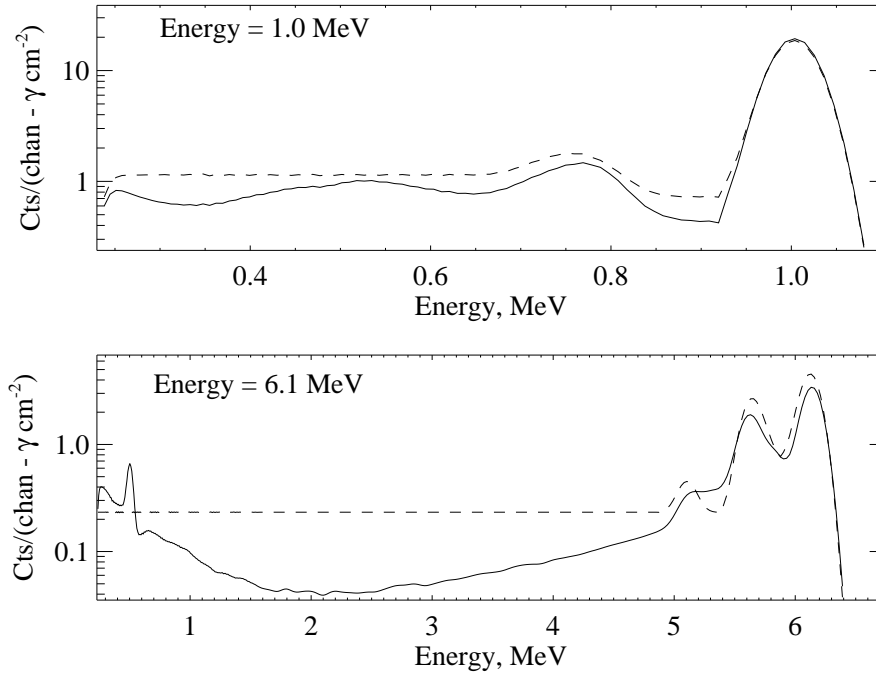


Figure 11. Comparison of the original GRS empirical instrument response (dashed curve) with the Monte Carlo derived response (solid curve) for lines at 1.0 and 6.1 MeV.

The detector response matrix (DRM) for *SMM* GRS, developed empirically before the launch of the satellite in 1980 (Forrest et al. 1980), has been used in studies of flares (e.g. Share & Murphy (1995); Vestrand et al. (1999)). As part of the current investigation we reevaluated the DRM using a Monte Carlo routine that was successfully applied to the OSSE instrument on the *Compton Gamma Ray Observatory* (*CGRO*) (Johnson et al. 1993). The GRS instrument was made of seven 7.6 cm diameter x 7.6 cm long cylindrical NaI (Tl) detectors in a close-packed array enclosed by an anti-coincidence system. The anti-coincidence system was made up of

four elements: a 2.54 cm thick CsI annulus made in four sections, a 7.6 cm thick CsI plate below the NaI detectors, a plastic detector above these detectors, and one below the CsI plate. In our simulations we assumed that the CsI detectors rejected any events with energy losses >100 keV. We also simulated the effects of gamma-ray scattering from a massive aluminum spacecraft and allowed for leakage through the anti-coincidence system that would be expected from the spaces between the various elements.

In Figure 11 we plot a comparison of the newly-adopted and original-empirical DRMs for incident photons of 1 and 6 MeV. The most significant differences occur for photon energies above an MeV where the new photo- and escape-peak efficiencies are slightly lower and the Compton-scattered continuum is significantly reduced. We believe that the large amount of continuum in the previous DRM, below ~ 5 MeV for 6.1 MeV photons in the lower plot, originated from uncorrected room-scattered radiation from radioactive sources used in the original calibration process.

B. ‘ELECTRON-DOMINATED’ EPISODES

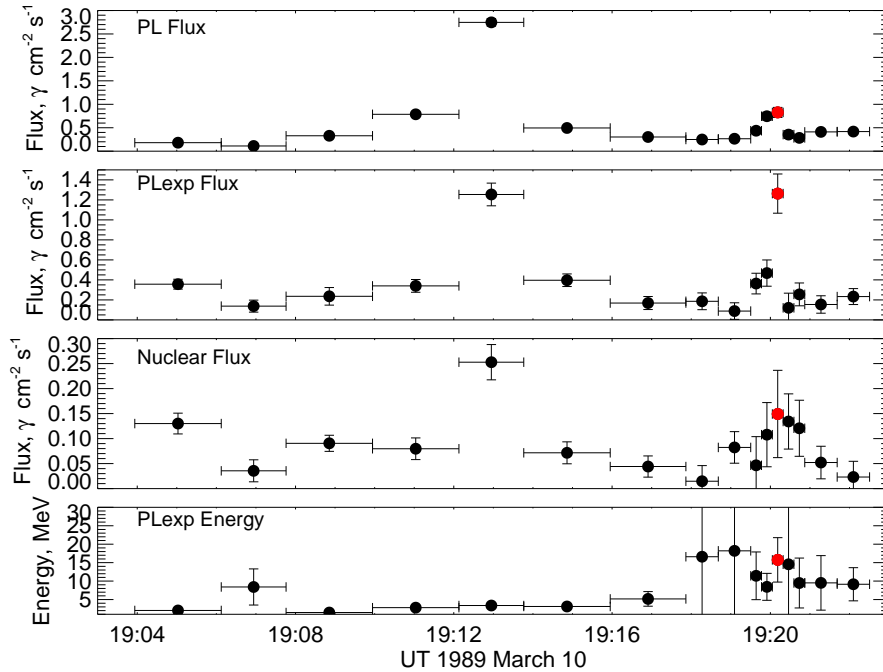


Figure 12. Time histories of the PL, PLexp, and nuclear fluxes, and the exponential rollover energy, E_R determined by fits to the 1989 March 10 flare prior to and during the 8-s ‘electron-dominated’ episode reported by [Rieger et al. \(1998\)](#). The red-filled circles denote the measurements made during the 16-s spectral accumulation that included the 8-s episode.

One way to reveal flare electrons at MeV energies is to search for times in flares when the nuclear emission is relatively weak. [Rieger et al. \(1998\)](#) reviewed 12 such events that they called ‘electron-dominated’ episodes. These events exhibit a flattening in the MeV continuum followed by rollovers at energies as high as several tens of MeV

in the spectra of some time intervals. Such features cannot be explained by transport effects alone (Petrosian et al. 1994) and therefore must be intrinsic to the acceleration mechanism. Park et al. (1997) showed that these features can be explained using models based on stochastic acceleration by turbulence, once loss mechanisms are properly included. Alternatively, Litvinenko (2000) demonstrated that electrons can be preferentially accelerated over protons to MeV energies, and above, in reconnecting current sheets.

Here we study the spectra of these ‘electron-dominated’ episodes to determine how the PL, PLe_{xp} and nuclear components compare with those observed in nuclear line flares. We begin our discussion of these events with the 8-s episode that occurred late in the 1989 March 10 flare. Notably, this flare is one of the 25 with nuclear lines in our study (Table 1). We accumulated spectra over different durations to reveal both the general evolution of the flare and the details of the episode. In Figure 12 we see that the PL, PLe_{xp}, and nuclear fluxes followed one another through the primary peak of the flare at 19:13 UT. However, while the PL and nuclear fluxes rose together to an unremarkable ~50-s long peak beginning at ~19:19 UT, the PLe_{xp} flux increased abruptly by a factor of three in the 16-s spectral accumulation that included the 8-s ‘electron-dominated’ episode. During this 16-s accumulation, the PLe_{xp} component had a rollover energy, E_R , of ~15 MeV, six times higher than the average for the entire flare (Table 1). These observations indicate that the ‘electron-dominated’ episode in this flare was mostly due to the abrupt increase in the flux and exponential rollover energy of the PLe_{xp} component. There was no evidence for a decrease in the nuclear emission during this episode.

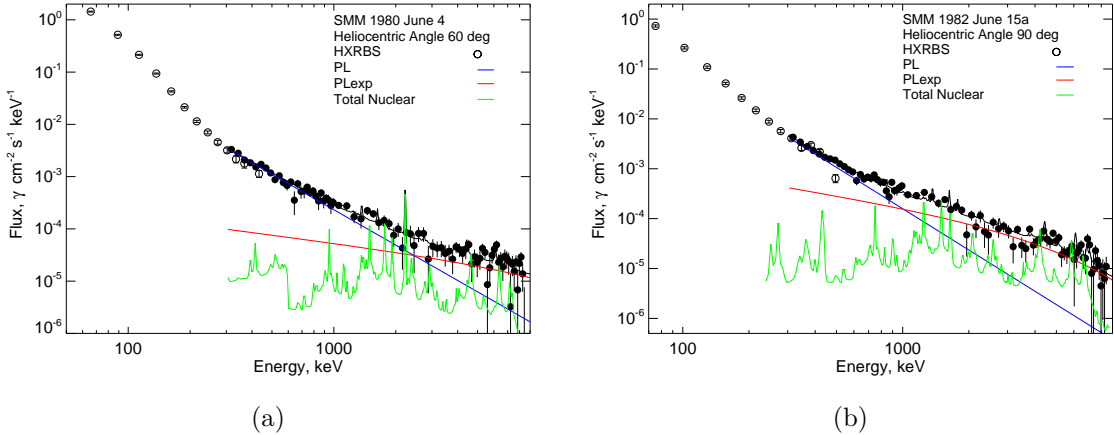


Figure 13. Combined *SMM* HXRBS and GRS spectra of two ‘electron-dominated’ episodes (Rieger et al. 1998): (a) the 48-s long 1980 June 4 flare discussed by Dennis (1988) and (b) the 84-s long flare on 1982 June 15. The three fitted components are plotted by the colored traces listed in the legends.

In Figure 13 we plot photon spectra from 60 keV to 8.5 MeV for two ‘electron-dominated’ flares listed in Rieger et al. (1998) using HXRBS and GRS data. As we

found for the three flares plotted in Figure 2, there is good agreement between the two instruments in their overlapping energy range. The PLe_{exp} component is clearly dominant at energies $\gtrsim 2$ MeV in both episodes with rollover energies of ~ 15 and 6 MeV. There is also a significant flux of nuclear γ rays in both episodes. Notably, there is something different about the hard X-ray spectra measured by HXRBS in these two flares compared with those plotted in Figure 2. In addition to the rollover in the spectra between 100 and 200 keV, both flares show evidence for hardening $\gtrsim 300$ keV not observed in the other spectra. We discuss a possible explanation for this hardening in Appendix E.

C. WEAK SOLAR FLARES

We studied the spectral characteristics of weak events by identifying 48 flares in the *SMM*/GRS catalog (Vestrand et al. 1999) with no detectable emission above 1 MeV. Because of the excellent gain stability of GRS (Forrest et al. 1980), it is possible to sum up the spectra from these flares over the entire 9.5-year mission without significant degradation in spectral resolution.

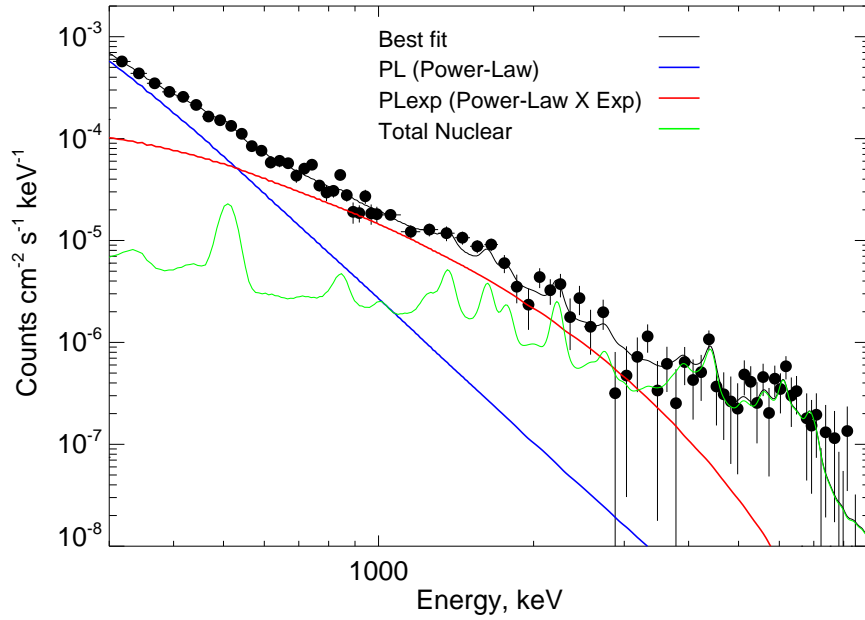


Figure 14. Summed spectrum from 48 flares observed by *SMM*/GRS each having no detectable emission >1 MeV. The fitted PL, PLe_{exp}, and nuclear components are plotted and defined in the legend. We used broader energy bins at high energies to improve statistics.

In Figure 14 we plot the summed count spectrum of these 48 flares. With the improved statistics at high energy from this summation we see that the spectrum of these weak flares clearly extends up to the 8.5 MeV maximum energy measured by GRS. Share & Murphy (2000) presented a similar spectrum from weak flares but

did not have the improved instrument response and nuclear templates to properly fit the data. Our fit to the summed spectrum reveals a PL component (blue line) that dominates below 500 keV and has an index of ~ 3.5 , the same as the mean index of the 25 large flares studied in this paper. The fit also reveals clear evidence for both the PLe_{exp} (red curve) and nuclear-line (green curve) components found in the more intense flares. What we find surprising is the absence of a significant 2.223-MeV neutron-capture line. The 2.223-MeV/nuclear de-excitation line flux ratio is 0.01 ± 0.006 in the sum of 48 weak flares. This is a factor of 40 smaller than the ratio observed in the 25 nuclear-line flares. Because the cross section for producing the neutron-capture line peaks at a higher-energy than the cross-sections for producing nuclear de-excitation lines, such a reduction in 2.223-MeV flux suggests that the ion spectrum in weak flares is significantly steeper than in larger flares.

D. POWER-LAW ELECTRON-PRODUCED VS ION-PRODUCED γ -RAY FLUENCE CORRELATIONS

Shih et al. (2009) analyzed a large sample of *RHESSI* and *SMM* flares and found a close correlation between the >300 keV electron bremsstrahlung fluence and 2.223 MeV neutron-capture line fluence from ion reactions over three orders of magnitude. Earlier studies revealed the close correlation between electron bremsstrahlung and nuclear de-excitation line fluences (Vestrand 1988; Murphy et al. 1993). These correlations indicate that accelerated electrons with energies >300 keV and protons with energies $\gtrsim 2$ MeV have a related origin.

We repeated these earlier comparisons using the angle-corrected PL and the nuclear de-excitation line fluences in 20 of the large flares at heliocentric angles $<85^\circ$.⁵ The results of this comparison are plotted as red-filled circles in Figure 15. We extended the plot to much weaker fluences using the summed spectra of the 48 weak flares (blue-filled circles) discussed in § C and 15 flares that were individually detected with weak emission >1 MeV (green-filled circles). The fluences of the ‘electron dominated’ episodes fill in the intermediate region. With these measurements, we see that the nuclear-line and PL fluences are correlated over almost three orders of magnitude.

E. SUBMILLIMETER AND GAMMA-RAY EVIDENCE FOR MEV ELECTRONS

As pointed out by Krucker et al. (2013) a combination of free–free absorption and Razin suppression is also capable of producing the submillimeter emission observed in flares. To produce the $>10^4$ SFU observed in the submillimeter band requires sources with linear dimension >20 arcsec, thermal electron densities $> 10^{12}$ cm⁻³, and temperatures near 10^6 K (Fleishman & Kontar 2010). One would need a significant source of heat deep in the chromosphere with cooler dense absorbing material along the line of sight. 5 MeV electrons can penetrate the chromosphere to hydrogen densities of 10^{16} cm⁻³ even when they are constrained in turbulent magnetic loops

⁵ We restricted the sample to avoid bremsstrahlung attenuation effects at the limb.

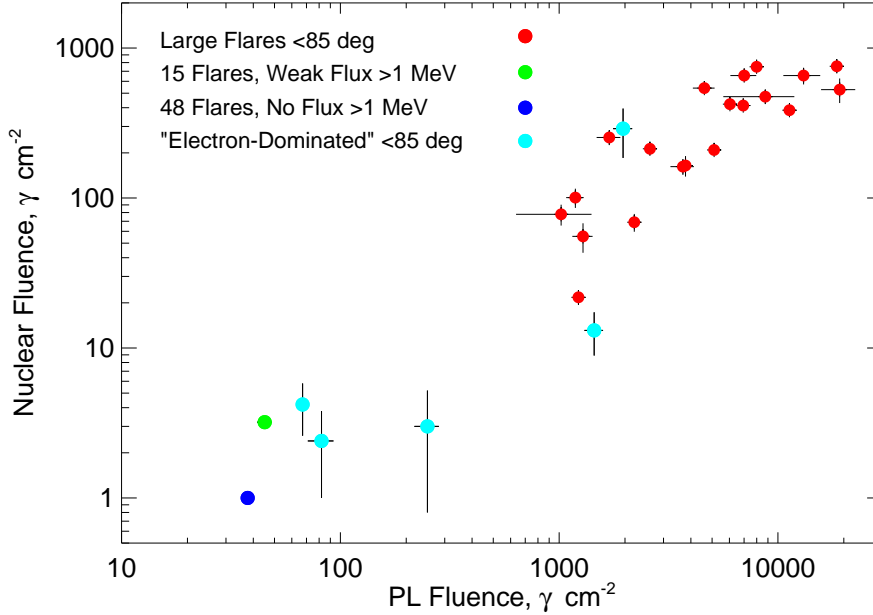


Figure 15. Plot of the nuclear de-excitation line *vs* the angle-corrected PL fluences for flares. Plotted are the fluences from 20 nuclear-line flares (red), 5 ‘electron-dominated’ episodes, the average fluence of the sum of 15 flares (green), each with only weak flux detected >1 MeV, and the average fluence of the sum of 48 flares (blue), each with no detectable flux >1 MeV.

(Miller & Ramaty 1989). Assuming a coronal source region with $n_h = 10^{11} \text{ cm}^{-3}$, a cubic volume of linear size $5 \times 10^7 \text{ cm}$, and a typical normalization factor of $5 \times 10^{53} \text{ cm}^{-2} \text{ s}^{-1}$ from our thin-target fits, we estimate that the flux of coronal electrons is $\sim 5 \times 10^{19} \text{ cm}^{-2} \text{ s}^{-1}$. For 5 MeV electrons this equates to an energy flux of $4 \times 10^{14} \text{ ergs cm}^{-2} \text{ s}^{-1}$.

We can estimate an upper limit on radiative losses by assuming that they are proportional to the product of n_h and n_e as they are in the corona (Raymond et al. 1976). Vernazza et al. (1981) estimated that the chromospheric radiative loss at $n_h = 10^{14} \text{ cm}^{-3}$ is $\sim 0.1 \text{ ergs cm}^{-3} \text{ s}^{-1}$. Assuming a density of 10^{16} cm^{-3} where the electrons lose most of their energy, the volume loss rate could then be as high as $\sim 1000 \text{ ergs cm}^{-3} \text{ s}^{-1}$. Assuming a volume with a thickness of 200 km the radiative loss in the Model C atmosphere could be as high as $2 \times 10^{10} \text{ ergs cm}^{-2} \text{ s}^{-1}$. This is about four orders of magnitude less than the energy flux imparted by the 5 MeV electrons. As the plasma temperature rises and it becomes fully ionized, the radiative losses could increase by as much as 10^4 making the input energy rate and upper limit on radiative losses comparable. Thus, it is possible that a fraction of the electrons from the new coronal source may be responsible for heating the chromosphere to temperatures high enough to produce submillimeter radiation.

Share et al. (2004) suggested that plasma at $\sim 5 \times 10^5 \text{ K}$ temperatures could explain the puzzling broadening of the 511 keV positron annihilation line observed at

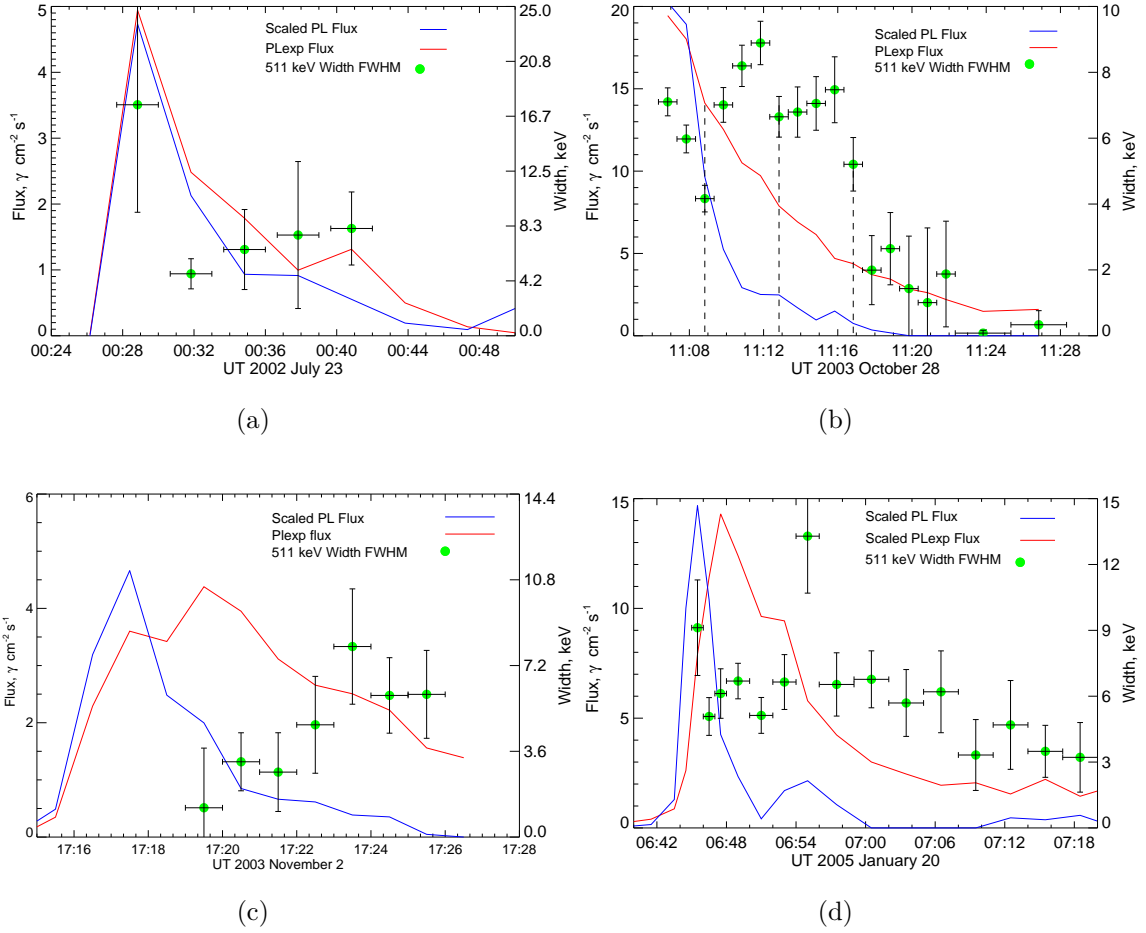


Figure 16. Comparison of the time histories of the PL and PLeXP fluxes and the 511 keV width (FWHM) in the spectra of 4 *RHESSI* flares.

times in flares. If MeV electrons from the new coronal source can heat the chromosphere to temperatures high enough to produce submillimeter radiation, they also could be responsible for broadening the line. Positrons are released in β -decays of radioactive nuclei produced by the interaction of flare-accelerated ions with chromospheric material at densities of 10^{14} to 10^{15} cm^{-3} . We therefore wish to determine if the width of the 511 keV line is correlated with the intensity of the coronal MeV electrons, as reflected in the PLeXP flux. In Figure 16 we compared the time histories of the PL and PLeXP photon fluxes and the width of the 511 keV line in four flares observed by *RHESSI*. The width in the 2002 July 23 flare appears to be broadened throughout the flare and followed the intensity variations in both the PL and PLeXP components. While the PL component in the 2003 October 28 flare fell rapidly after 11:08 UT, the PLeXP component remained at 25% of its peak value until 11:16 UT when the 511 keV line narrowed significantly. Schrijver et al. (2006) found anomalies in magnetograms and UV ribbons during this flare that persisted up to ~ 5 min and are consistent a warm, dense medium that would broaden the 511 keV line. In both

the 2003 November 2 and 2005 January 20 flares the PL component again dissipated rapidly, while the PLe_{exp} component persisted, possibly providing the energy to heat the plasma sufficiently to cause the 511 keV line to broaden after 17:23 UT in the November flare and to sustain the broad line until late in the January observation. This evidence for a correlation of the 511-keV line width and the PLe_{exp} flux is consistent with a source of MeV electrons that heats the chromosphere to $\sim 5 \times 10^5$ K temperatures.

Raymond et al. (2007) used *SOHO*/UVCS measurements of scattered O VI in the corona to infer the luminosities at transition regions temperatures in the 2002 July 23 flare. They found that the luminosities were consistent with being produced in a conventional but high density (e.g. 10^{12} cm⁻³) transition region 10 km thick. This measurement appears to be inconsistent with emission at the densities $> 10^{14}$ cm⁻³ where the positrons producing the annihilation line observed by *RHESSI* would likely annihilate because it would require very small transition region thicknesses of about 0.1 km. However, because passage of the CME disturbed the corona where the resonantly-scattered O VI was emitted, the UVCS observations effectively ended at the onset of the γ -ray emission (Johnson et al. 2011). The UVCS measurements for the 2003 November 2 flare also ended minutes before the 511 keV line was observed to broaden. Another consideration is that 5 MeV electrons lose most of their energy near the end of their range and this layer is only ~ 2 km thick, approaching the thicknesses required for O VI luminosities observed if the emission came from deep in the chromosphere.

One might wonder why these high-energy electrons do not produce an observable flux of MeV γ rays from thick-target bremsstrahlung at the footpoints of the flares. Such high-energy bremsstrahlung is strongly downward beamed (Petrosian 1985) and only the lower energy upward-scattered photons escape the solar atmosphere. This flat spectrum would be difficult to detect against the accompanying steep spectrum of hard X-rays from the footpoints. However, during times when the flux of MeV electrons is especially enhanced, such as during ‘electron-dominated’ episodes, bremsstrahlung from these MeV electrons might be detectable. In Figure 13(a) and (b) we plotted combined *SMM*HXRBS and GRS spectra from two ‘electron-dominated’ flares which exhibit hardening near 300 keV not observed in other flare spectra. We offer the possibility that this hardening is evidence for up-scattered bremsstrahlung from coronal MeV electrons that reach the chromosphere.

REFERENCES

- | | |
|---|---|
| <p>Ackermann, M., Ajello, M., Allafort, A.,
et al. 2012, <i>ApJ</i>, 745, 144,
doi: 10.1088/0004-637X/745/2/144</p> | <p>Ajello, M., Baldini, L., Bastieri, D., et al.
2021, <i>ApJS</i>, 252, 13,
doi: 10.3847/1538-4365/abd32e</p> <p>Bai, T., & Ramaty, R. 1976, <i>SoPh</i>, 49,
343, doi: 10.1007/BF00162457</p> |
|---|---|

- Bastian, T. S., Benz, A. O., & Gary, D. E. 1998, *ARA&A*, 36, 131, doi: [10.1146/annurev.astro.36.1.131](https://doi.org/10.1146/annurev.astro.36.1.131)
- Benz, A. O. 2017, *Living Reviews in Solar Physics*, 14, 2, doi: [10.1007/s41116-016-0004-3](https://doi.org/10.1007/s41116-016-0004-3)
- Blumenthal, G. R., & Gould, R. J. 1970, *Reviews of Modern Physics*, 42, 237, doi: [10.1103/RevModPhys.42.237](https://doi.org/10.1103/RevModPhys.42.237)
- Chen, B., & Bastian, T. S. 2012, *ApJ*, 750, 35, doi: [10.1088/0004-637X/750/1/35](https://doi.org/10.1088/0004-637X/750/1/35)
- Chen, B., Shen, C., Gary, D. E., et al. 2020, *Nature Astronomy*, 4, 1140, doi: [10.1038/s41550-020-1147-7](https://doi.org/10.1038/s41550-020-1147-7)
- Chupp, E. L., Forrest, D. J., Higbie, P. R., et al. 1973, *Nature*, 241, 333, doi: [10.1038/241333a0](https://doi.org/10.1038/241333a0)
- Dennis, B. R. 1988, *SoPh*, 118, 49, doi: [10.1007/BF00148588](https://doi.org/10.1007/BF00148588)
- Ellison, D. C., & Ramaty, R. 1985, *ApJ*, 298, 400, doi: [10.1086/163623](https://doi.org/10.1086/163623)
- Fenimore, E. E., Klebesadel, R. W., & Laros, J. G. 1983, *Advances in Space Research*, 3, 207, doi: [10.1016/0273-1177\(83\)90032-7](https://doi.org/10.1016/0273-1177(83)90032-7)
- Fleishman, G. D., Gary, D. E., Chen, B., et al. 2020, *Science*, 367, 278, doi: [10.1126/science.aax6874](https://doi.org/10.1126/science.aax6874)
- Fleishman, G. D., & Kontar, E. P. 2010, *ApJL*, 709, L127, doi: [10.1088/2041-8205/709/2/L127](https://doi.org/10.1088/2041-8205/709/2/L127)
- Fletcher, L., Dennis, B. R., Hudson, H. S., et al. 2011, *SSRv*, 159, 19, doi: [10.1007/s11214-010-9701-8](https://doi.org/10.1007/s11214-010-9701-8)
- Forrest, D. J., Vestrand, W. T., Chupp, E. L., Rieger, E., & Cooper, J. 1986, *Advances in Space Research*, 6, 115, doi: [10.1016/0273-1177\(86\)90127-4](https://doi.org/10.1016/0273-1177(86)90127-4)
- Forrest, D. J., Chupp, E. L., Ryan, J. M., et al. 1980, *SoPh*, 65, 15, doi: [10.1007/BF00151381](https://doi.org/10.1007/BF00151381)
- Haug, E. 1998, *SoPh*, 178, 341, doi: [10.1023/A:1005098624121](https://doi.org/10.1023/A:1005098624121)
- Holman, G. D. 1985, *ApJ*, 293, 584, doi: [10.1086/163263](https://doi.org/10.1086/163263)
- Holman, G. D., & Benka, S. G. 1992, *ApJL*, 400, L79, doi: [10.1086/186654](https://doi.org/10.1086/186654)
- Holman, G. D., Aschwanden, M. J., Aurass, H., et al. 2011, *SSRv*, 159, 107, doi: [10.1007/s11214-010-9680-9](https://doi.org/10.1007/s11214-010-9680-9)
- Hua, X.-M., & Lingenfelter, R. E. 1987, *SoPh*, 107, 351, doi: [10.1007/BF00152031](https://doi.org/10.1007/BF00152031)
- Hua, X.-M., Ramaty, R., & Lingenfelter, R. E. 1989, *ApJ*, 341, 516, doi: [10.1086/167513](https://doi.org/10.1086/167513)
- Johnson, H., Raymond, J. C., Murphy, N. A., et al. 2011, *ApJ*, 735, 70, doi: [10.1088/0004-637X/735/2/70](https://doi.org/10.1088/0004-637X/735/2/70)
- Johnson, W. N., Kinzer, R. L., Kurfess, J. D., et al. 1993, *ApJS*, 86, 693, doi: [10.1086/191795](https://doi.org/10.1086/191795)
- Jones, F. C. 1968, *Physical Review*, 167, 1159, doi: [10.1103/PhysRev.167.1159](https://doi.org/10.1103/PhysRev.167.1159)
- Kaufmann, P., Trottet, G., Giménez de Castro, C. G., et al. 2009, *SoPh*, 255, 131, doi: [10.1007/s11207-008-9312-7](https://doi.org/10.1007/s11207-008-9312-7)
- Kaufmann, P., Raulin, J.-P., de Castro, C. G. G., et al. 2004, *ApJL*, 603, L121, doi: [10.1086/383186](https://doi.org/10.1086/383186)
- Kontar, E. P., Emslie, A. G., Massone, A. M., et al. 2007, *ApJ*, 670, 857, doi: [10.1086/521977](https://doi.org/10.1086/521977)
- Kontar, E. P., Jeffrey, N. L. S., & Emslie, A. G. 2019, *ApJ*, 871, 225, doi: [10.3847/1538-4357/aafad3](https://doi.org/10.3847/1538-4357/aafad3)
- Kontar, E. P., Brown, J. C., Emslie, A. G., et al. 2011, *SSRv*, 159, 301, doi: [10.1007/s11214-011-9804-x](https://doi.org/10.1007/s11214-011-9804-x)
- Kozlovsky, B., Murphy, R. J., & Ramaty, R. 2002, *ApJS*, 141, 523, doi: [10.1086/340545](https://doi.org/10.1086/340545)
- Krucker, S., Hurford, G. J., MacKinnon, A. L., Shih, A. Y., & Lin, R. P. 2008a, *ApJL*, 678, L63, doi: [10.1086/588381](https://doi.org/10.1086/588381)
- Krucker, S., Battaglia, M., Cargill, P. J., et al. 2008b, *A&A Rv*, 16, 155, doi: [10.1007/s00159-008-0014-9](https://doi.org/10.1007/s00159-008-0014-9)
- Krucker, S., Giménez de Castro, C. G., Hudson, H. S., et al. 2013, *A&A Rv*, 21, 58, doi: [10.1007/s00159-013-0058-3](https://doi.org/10.1007/s00159-013-0058-3)
- Kurt, V. G., Yushkov, B. Y., Galkin, V. I., Kudela, K., & Kashapova, L. K. 2017, *NewA*, 56, 102, doi: [10.1016/j.newast.2017.05.002](https://doi.org/10.1016/j.newast.2017.05.002)

- Leibacher, J., Sakurai, T., Schrijver, C. J., & van Driel-Gesztelyi, L. 2010, *SoPh*, 263, 1, doi: [10.1007/s11207-010-9553-0](https://doi.org/10.1007/s11207-010-9553-0)
- Lin, R. P., & Schwartz, R. A. 1987, *ApJ*, 312, 462, doi: [10.1086/164891](https://doi.org/10.1086/164891)
- Lin, R. P., Dennis, B. R., Hurford, G. J., et al. 2002, *SoPh*, 210, 3, doi: [10.1023/A:1022428818870](https://doi.org/10.1023/A:1022428818870)
- Litvinenko, Y. E. 2000, *SoPh*, 194, 327, doi: [10.1023/A:1005298816626](https://doi.org/10.1023/A:1005298816626)
- Lüthi, T., Lüdi, A., & Magun, A. 2004, *A&A*, 420, 361, doi: [10.1051/0004-6361:20035899](https://doi.org/10.1051/0004-6361:20035899)
- Lysenko, A. L., Anfinogentov, S. A., Svinkin, D. S., Frederiks, D. D., & Fleishman, G. D. 2019, *ApJ*, 877, 145, doi: [10.3847/1538-4357/ab1be0](https://doi.org/10.3847/1538-4357/ab1be0)
- MacKinnon, A., Szpigel, S., Gimenez de Castro, G., & Tuneu, J. 2020, *SoPh*, 295, 174, doi: [10.1007/s11207-020-01699-9](https://doi.org/10.1007/s11207-020-01699-9)
- MacKinnon, A. L., & Mallik, P. C. V. 2010, *A&A*, 510, A29, doi: [10.1051/0004-6361/200913190](https://doi.org/10.1051/0004-6361/200913190)
- Meegan, C., Lichti, G., Bhat, P. N., et al. 2009, *ApJ*, 702, 791, doi: [10.1088/0004-637X/702/1/791](https://doi.org/10.1088/0004-637X/702/1/791)
- Miller, J. A., & Ramaty, R. 1989, *ApJ*, 344, 973, doi: [10.1086/167865](https://doi.org/10.1086/167865)
- Murphy, R., & Share, G. 2018, *SoPh*, 293, 163, doi: [10.1007/s11207-018-1386-2](https://doi.org/10.1007/s11207-018-1386-2)
- Murphy, R. J., Dermer, C. D., & Ramaty, R. 1987, *ApJS*, 63, 721, doi: [10.1086/191180](https://doi.org/10.1086/191180)
- Murphy, R. J., Kozlovsky, B., Kiener, J., & Share, G. H. 2009, *ApJS*, 183, 142, doi: [10.1088/0067-0049/183/1/142](https://doi.org/10.1088/0067-0049/183/1/142)
- Murphy, R. J., Kozlovsky, B., & Share, G. H. 2012, *ApJS*, 202, 3, doi: [10.1088/0067-0049/202/1/3](https://doi.org/10.1088/0067-0049/202/1/3)
- . 2014, *ApJS*, 215, 18, doi: [10.1088/0067-0049/215/2/18](https://doi.org/10.1088/0067-0049/215/2/18)
- . 2016, *ApJ*, 833, 196, doi: [10.3847/1538-4357/833/2/196](https://doi.org/10.3847/1538-4357/833/2/196)
- Murphy, R. J., Kozlovsky, B., Share, G. H., Hua, X., & Lingenfelter, R. E. 2007, *ApJS*, 168, 167, doi: [10.1086/509637](https://doi.org/10.1086/509637)
- Murphy, R. J., Share, G. H., Skibo, J. G., & Kozlovsky, B. 2005, *ApJS*, 161, 495, doi: [10.1086/452634](https://doi.org/10.1086/452634)
- Murphy, R. J., Share, G. H., Grove, J. E., et al. 1993, in *American Institute of Physics Conference Series*, Vol. 280, American Institute of Physics Conference Series, ed. M. Friedlander, N. Gehrels, & D. J. Macomb, 619–630
- Ohki, K., & Hudson, H. S. 1975, *SoPh*, 43, 405, doi: [10.1007/BF00152364](https://doi.org/10.1007/BF00152364)
- Oparin, I. D., Charikov, Y. E., Ovchinnikova, E. P., & Shabalin, A. N. 2020, *Geomagnetism and Aeronomy*, 60, 889, doi: [10.1134/S0016793220070191](https://doi.org/10.1134/S0016793220070191)
- Orwig, L. E., Frost, K. J., & Dennis, B. R. 1980, *SoPh*, 65, 25, doi: [10.1007/BF00151382](https://doi.org/10.1007/BF00151382)
- Park, B. T., Petrosian, V., & Schwartz, R. A. 1997, *ApJ*, 489, 358, doi: [10.1086/304753](https://doi.org/10.1086/304753)
- Petrosian, V. 1985, *ApJ*, 299, 987, doi: [10.1086/163765](https://doi.org/10.1086/163765)
- Ramaty, R., Kozlovsky, B., & Lingenfelter, R. E. 1979, *ApJS*, 40, 487, doi: [10.1086/190596](https://doi.org/10.1086/190596)
- Ramaty, R., Kozlovsky, B., & Suri, A. N. 1977, *ApJ*, 214, 617, doi: [10.1086/155288](https://doi.org/10.1086/155288)
- Raymond, J. C., Cox, D. P., & Smith, B. W. 1976, *ApJ*, 204, 290, doi: [10.1086/154170](https://doi.org/10.1086/154170)
- Raymond, J. C., Holman, G., Ciaravella, A., et al. 2007, *ApJ*, 659, 750, doi: [10.1086/512604](https://doi.org/10.1086/512604)
- Rieger, E., Gan, W. Q., & Marschhäuser, H. 1998, *SoPh*, 183, 123, doi: [10.1023/A:1005060921400](https://doi.org/10.1023/A:1005060921400)
- Rieger, E., Reppin, C., Kanbach, G., et al. 1983, *International Cosmic Ray Conference*, 10, 338
- Schrijver, C. J., Hudson, H. S., Murphy, R. J., Share, G. H., & Tarbell, T. D. 2006, *ApJ*, 650, 1184, doi: [10.1086/506583](https://doi.org/10.1086/506583)
- Share, G. H., Murphy, R., Grove, J. E., & Shih, A. Y. 2022, in *AGU Fall Meeting Abstracts*, Vol. 2022, SH43A–03
- Share, G. H., & Murphy, R. J. 1995, *ApJ*, 452, 933, doi: [10.1086/176360](https://doi.org/10.1086/176360)

- Share, G. H., & Murphy, R. J. 2000, in American Institute of Physics Conference Series, Vol. 528, Acceleration and Transport of Energetic Particles Observed in the Heliosphere, ed. R. A. Mewaldt, J. R. Jokipii, M. A. Lee, E. Möbius, & T. H. Zurbuchen, 181–184
- Share, G. H., Murphy, R. J., Kiener, J., & de Séréville, N. 2002, *ApJ*, 573, 464, doi: [10.1086/340595](https://doi.org/10.1086/340595)
- Share, G. H., Murphy, R. J., Smith, D. M., Schwartz, R. A., & Lin, R. P. 2004, *ApJL*, 615, L169, doi: [10.1086/426478](https://doi.org/10.1086/426478)
- Share, G. H., Murphy, R. J., White, S. M., et al. 2018, *ApJ*, 869, 182, doi: [10.3847/1538-4357/aaebf7](https://doi.org/10.3847/1538-4357/aaebf7)
- Shih, A. Y., Lin, R. P., & Smith, D. M. 2009, *ApJL*, 698, L152, doi: [10.1088/0004-637X/698/2/L152](https://doi.org/10.1088/0004-637X/698/2/L152)
- Silva, A. V. R., Share, G. H., Murphy, R. J., et al. 2007, *SoPh*, 245, 311, doi: [10.1007/s11207-007-9044-0](https://doi.org/10.1007/s11207-007-9044-0)
- Smith, D. M., Share, G. H., Murphy, R. J., et al. 2003, *ApJL*, 595, L81, doi: [10.1086/378173](https://doi.org/10.1086/378173)
- Suri, A. N., Chupp, E. L., Forrest, D. J., & Reppin, C. 1975, *SoPh*, 43, 415, doi: [10.1007/BF00152365](https://doi.org/10.1007/BF00152365)
- Trottet, G., Krucker, S., Lüthi, T., & Magun, A. 2008, *ApJ*, 678, 509, doi: [10.1086/528787](https://doi.org/10.1086/528787)
- Tusnski, D. S., Szpigel, S., Giménez de Castro, C. G., MacKinnon, A. L., & Simões, P. J. A. 2019, *SoPh*, 294, 103, doi: [10.1007/s11207-019-1499-2](https://doi.org/10.1007/s11207-019-1499-2)
- Vernazza, J. E., Avrett, E. H., & Loeser, R. 1981, *ApJS*, 45, 635, doi: [10.1086/190731](https://doi.org/10.1086/190731)
- Vestrand, W. T. 1988, *SoPh*, 118, 95, doi: [10.1007/BF00148589](https://doi.org/10.1007/BF00148589)
- Vestrand, W. T., Forrest, D. J., Chupp, E. L., Rieger, E., & Share, G. H. 1987, *ApJ*, 322, 1010, doi: [10.1086/165796](https://doi.org/10.1086/165796)
- Vestrand, W. T., & Ghosh, A. 1987, in International Cosmic Ray Conference, Vol. 3, International Cosmic Ray Conference, 57
- Vestrand, W. T., Share, G. H., Murphy, R. J., et al. 1999, *ApJS*, 120, 409, doi: [10.1086/313180](https://doi.org/10.1086/313180)
- Vilmer, N., MacKinnon, A. L., & Hurford, G. J. 2011, *SSRv*, 159, 167, doi: [10.1007/s11214-010-9728-x](https://doi.org/10.1007/s11214-010-9728-x)
- White, S. M., Benz, A. O., Christe, S., et al. 2011, *SSRv*, 159, 225, doi: [10.1007/s11214-010-9708-1](https://doi.org/10.1007/s11214-010-9708-1)